

Characterization of Multi-Pixel Photon Counters for a new neutrino detector

Fuminao Hosomi

The University of Tokyo, Department of Physics, Tokyo, Japan

February 3, 2016

Abstract

We have been developing a new neutrino detector named WAGASCI, to measure the cross section ratio of neutrino interaction with water and hydrocarbon by using the J-PARC neutrino beam. The optical crosstalk suppression type Multi-Pixel Photon Counters (MPPCs) by Hamamatsu is newly developed to be used in the WAGASCI detector. The new MPPC has an order of magnitude lower dark noise rate and optical crosstalk than earlier devices, and can be operated with higher over voltage, which results in higher photon detection efficiency (PDE).

The WAGASCI detector will have a large number of readout channels. In order to realize a compact readout with a large number of channels, we developed an array of 32 MPPCs. A characterization system to measure a large number of MPPCs is being developed. The gain, relative PDE, dark noise rate, and optical crosstalk will be measured for different temperature and over voltage. The performance of 64 single channel MPPCs or four arrays of MPPC (i.e. 128 channels) will be simultaneously and automatically measured by using the characterization system. The measurement of the gain and relative PDE of 64 MPPCs with operating MPPCs for the reference already succeeded.

In this thesis, the performance of the optical crosstalk suppression type MPPC and the development of the characterization system are reported.

Acknowledgments

I would like to express my sincere gratitude to my supervisor, Prof. Masashi Yokoyama. When I come up against difficulties with the research, he always gives practical advice that inspires me to further efforts. Without his guidance and persistent help, this thesis would not have been achieved.

I am cordially grateful to WAGASCI colleagues for many helps in my work. Dr. Akihiro Minamino gives me tremendous support and warm encouragement. I owe a great debt to Prof. Nakaya Tsuyoshi, Prof. Yoshihiro Seiya, Prof. Atsuko Ichikawa, Prof. Kazuhiro Yamamoto, Prof. Yoshinari Hayato, and Dr. Benjamin Quilain for insightful comments and suggestions. Many thanks go to Taichiro Koga, Naruhiro Chikuma, Tatsuya Hayashino, Keigo Nakamura, Ken'ichi Kin, Jun Harada, Tatiana Ovsianikova, and Liccialdi Matthieu. I spent my wonderful research life with them especially in Tokai.

I would like to show my heartfelt appreciation to the member in our group of the University of Tokyo, Prof. Hiroaki Aihara, Dr. Yoshiyuki Onuki, Dr. Denis Epifanov, Dr. Ian Watson, Sogo Mineo, Clement Ng, Yusuke Suda, Nobuhiro Shimizu, Junya Sasaki, Yifan Jin, Hiroko Niikura, Tianmeng Lou, Mora Alejandro, and Wan Kun. They gave me useful advice and fruitful life in Hongo. I am also deeply thankful to the secretary of the University of Tokyo, Ms. Kuniko Kono for providing meticulous support through my college life.

The work of this thesis has been financially supported by Advanced Leading Graduate Course for Photon Science (ALPS) at the University of Tokyo. I strongly hope that more and more students in their master's course will be supported with non-refundable scholarship such as the ALPS course.

Special thanks go to all my friends, especially whom I met through orchestra and wind orchestra. Their *mental harmony* offers emotional support at all times when I am depressed and vivacious.

Finally, I would like to express profound gratitude to my parents and my brother for providing hearty support and cheerful play through my entire life.

Contents

1	Introduction	11
1.1	Neutrino oscillation	11
1.2	T2K experiment	12
1.2.1	J-PARC neutrino beam	12
1.2.2	Detectors	13
1.2.3	Current status and future prospects	13
1.3	WAGASCI experiment	14
1.3.1	Motivation	14
1.3.2	Location of the detector	14
1.3.3	Detector design	14
1.4	Contents of this thesis	17
2	Multi-Pixel Photon Counters	19
2.1	Avalanche Photodiode	19
2.1.1	Principle of avalanche multiplication	19
2.1.2	Geiger mode	21
2.2	Silicon Photomultiplier	22
2.3	Characteristics of MPPC	23
2.3.1	Gain	23
2.3.2	Photon detection efficiency	24
2.3.3	Dark noise	24
2.3.4	Optical crosstalk	24
2.3.5	Afterpulse	25
3	Development of MPPC	27
3.1	History of MPPC development	27
3.2	Performance of MPPC	27
3.2.1	Dark noise rate	28
3.2.2	Optical crosstalk	28
3.2.3	Gain	31
3.2.4	Relative PDE	32
3.2.5	Summary	33

4	Development of MPPC characterization system	35
4.1	Requirements	35
4.1.1	Outline	35
4.1.2	MPPCs used for the WAGASCI detector	35
4.2	Design of the characterization system	36
4.2.1	NIM EASIROC module	36
4.2.2	Temperature controlled chamber	38
4.2.3	Printed circuit board fixing MPPCs	39
4.2.4	Light source	39
4.2.5	Support structure	39
4.3	Measurement method	41
4.4	Performance of the characterization system	43
4.4.1	Light intensity	43
4.4.2	Performance of 64 MPPCs	48
5	Future prospects and summary	49
5.1	Future prospects	49
5.1.1	Light intensity	49
5.1.2	Dark noise and optical crosstalk	49
5.1.3	Temperature scan	50
5.1.4	Measurement of the MPPCs used in the WAGASCI detector	50
5.2	Summary	50
A	Wiring of the PCB for single channel MPPC	51

List of Figures

1.1	The overview of the T2K experiment.	12
1.2	A candidate site of the WAGASCI detector.	14
1.3	The expected neutrino energy spectrum at the candidate site of the WAGASCI detector and at the site of ND280	15
1.4	The configuration of WAGASCI detector.	15
1.5	The 3D grid-like structure of the 3-mm thick scintillators.	16
2.1	PN junction state of photodiodes.	20
2.2	Schematic diagram of avalanche multiplication.	20
2.3	The basic operation process of a combination of the APD operating in the Geiger mode and the quenching resistor.	22
2.4	Structure of the SiPM.	22
2.5	Picture of ceramic packaged MPPC.	23
3.1	Readout circuit used for performance test of MPPCs.	28
3.2	The waveforms of the three different MPPCs.	29
3.3	The micrographs of MPPCs.	29
3.4	The diagram of setup for measuring dark noise rate and optical crosstalk.	29
3.5	The results of the performance test for each MPPCs.	30
3.6	The diagram of setup for measuring gain and relative PDE.	31
3.7	A typical charge distribution of MPPC.	31
3.8	A picture of setup for measuring relative PDE.	32
3.9	Variation of measured relative PDE due to MPPC replacement.	32
4.1	An array of MPPCs.	36
4.2	The basic concept of characterization system.	36
4.3	Picture of NIM EASIROC module.	37
4.4	A schematic of one channel in EASIROC chip.	37
4.5	Temperature controlled chamber.	38
4.6	Pictures of PCB for MPPCs.	39
4.7	A Schematic of the light source.	40
4.8	A schematic of the LED driver.	40
4.9	Design of the support structure.	41
4.10	Picture when measuring single channel MPPCs.	41

4.11	Diagram of digital signals when operating characterization system with multiple EASIROC modules.	42
4.12	The layout mapping of 64 single channel MPPCs.	44
4.13	The gain and the number of detected photons of one MPPC.	45
4.14	The distribution of the light intensity in units of the number of detected photons when using the first version of light source.	45
4.15	The distribution of the light intensity in units of the number of detected photons when using the second version of light source.	46
4.16	The fluctuation of the mean of the number of photons detected by two MPPCs for the reference.	46
4.17	The light intensity distribution of ten times measurement without the correction by using the light intensity for the reference.	47
4.18	The light intensity distribution of ten times measurement with the correction by using the light intensity for the reference.	47
4.19	Performance of 64 MPPCs.	48
A.1	The wiring of anodes.	52
A.2	The wiring of cathodes.	52

List of Tables

- 1.1 Summary of the systematic uncertainties on the predicted event rate. 13
- 2.1 The characteristics of the APD operating in normal mode and Geiger mode. . . 21
- 3.1 Three types of MPPC measured in this study. 27
- 3.2 The comparison of the performance of MPPC. 33
- 4.1 Digital inputs and outputs of NIM EASIROC module 38

Chapter 1

Introduction

1.1 Neutrino oscillation

Neutrino is one of the elementary particles and classified into neutral leptons in the framework of the Standard Model. Three types of neutrinos are already discovered and known as electron neutrino (ν_e), muon neutrino (ν_μ), and tau neutrino (ν_τ). These types or flavors of neutrinos are related to corresponding charged leptons as the name indicates. These neutrinos are in a flavor eigenstate and can interact with charged leptons in weak interactions.

A neutrino created with a specific lepton flavor can later be measured to have a different flavor in a process known as neutrino oscillation. The first evidence for the neutrino oscillation was found by the Super-Kamiokande experiment [1] and by the SNO (Sudbury Neutrino Observatory) experiment [2].

The neutrino oscillation assumes that neutrinos have non-zero mass. Let ν_1 , ν_2 , and ν_3 be mass eigenstates of neutrinos that have mass of m_1 , m_2 , and m_3 . Neutrino flavor eigenstates are generally expressed as superposition of the mass eigenstates:

$$\begin{pmatrix} \nu_e \\ \nu_\mu \\ \nu_\tau \end{pmatrix} = U_{\text{PMNS}} \begin{pmatrix} \nu_1 \\ \nu_2 \\ \nu_3 \end{pmatrix}, \quad (1.1)$$

where U_{PMNS} is a 3×3 unitary matrix that is referred to as the Pontecorvo-Maki-Nakagawa-Sakata (PMNS) matrix [3, 4, 5, 6]. The matrix is expressed in terms of the three mixing angles, θ_{12} , θ_{23} , θ_{13} , and one complex phase δ_{CP} as

$$U_{\text{PMNS}} = \begin{pmatrix} 1 & 0 & 0 \\ 0 & c_{23} & s_{23} \\ 0 & -s_{23} & c_{23} \end{pmatrix} \begin{pmatrix} c_{13} & 0 & s_{13}e^{-i\delta_{CP}} \\ 0 & 1 & 0 \\ -s_{13}e^{i\delta_{CP}} & 0 & c_{13} \end{pmatrix} \begin{pmatrix} c_{12} & s_{12} & 0 \\ -s_{12} & c_{12} & 0 \\ 0 & 0 & 1 \end{pmatrix}, \quad (1.2)$$

where $c_{ij} = \cos \theta_{ij}$ and $s_{ij} = \sin \theta_{ij}$ ($i, j = 1, 2, 3$). In case of $\sin \delta_{CP} \neq 0$, the PMNS matrix includes the imaginary parts that causes the CP violation in the lepton sector.

The probabilities of $\nu_\alpha \rightarrow \nu_\beta$ ($\alpha, \beta = e, \mu, \tau$) oscillation is derived from Schrödinger equation

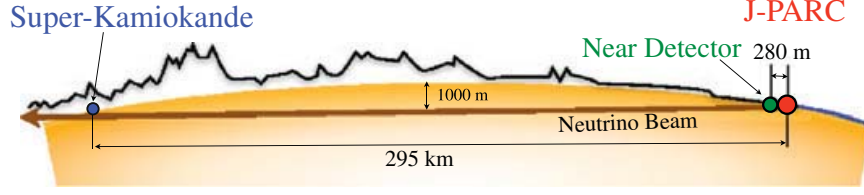


Figure 1.1: The overview of the T2K experiment. Neutrinos produced at J-PARC (red dot) fly through the near detectors (green dot) and arrive at Super-Kamiokande (blue dot) [7].

and expressed as

$$\begin{aligned}
 P(\nu_\alpha \rightarrow \nu_\beta) = & \delta_{\alpha\beta} - 4 \sum_{i>j} \Re(U_{\alpha i}^* U_{\beta i} U_{\alpha j} U_{\beta j}^*) \sin^2 \left(\frac{\Delta m_{ij}^2 L}{4E} \right) \\
 & + 2 \sum_{i>j} \Im(U_{\alpha i}^* U_{\beta i} U_{\alpha j} U_{\beta j}^*) \sin \left(\frac{\Delta m_{ij}^2 L}{2E} \right), \quad (1.3)
 \end{aligned}$$

where L , E , and $\Delta m_{ij}^2 = m_i^2 - m_j^2$ are the distance that a neutrino travels, the energy of the neutrino, and the squared mass difference of neutrinos, respectively.

1.2 T2K experiment

The T2K (Tokai to Kamioka) experiment is a long baseline neutrino oscillation experiment using neutrino beam produced at J-PARC (Japan Proton Accelerator Research Complex) [7]. The overview of the T2K experiment is illustrated in Fig 1.1. The T2K experiment sends an intense beam of muon neutrinos from Tokai to Kamioka at a distance of 295 km. The property of neutrinos is measured by near detectors in the J-PARC site and a far detector, Super-Kamiokande (SK) [8].

The main goal of T2K is the precise measurement of the neutrino oscillation. T2K have measured the probabilities of $\nu_\mu \rightarrow \nu_e$ appearance and $\nu_\mu \rightarrow \nu_\mu$ disappearance by using neutrino beam since T2K started in 2009 [9, 10]. In addition, the probabilities of $\bar{\nu}_\mu \rightarrow \bar{\nu}_e$ appearance and $\bar{\nu}_\mu \rightarrow \bar{\nu}_\mu$ disappearance have been measured by using anti-neutrino beam since 2014 [11]. The further precise measurement of the neutrino oscillation leads to a search for CP violation in the lepton sector by comparing the probabilities of $\nu_\mu \rightarrow \nu_e$ appearance and $\bar{\nu}_\mu \rightarrow \bar{\nu}_e$ appearance [12].

1.2.1 J-PARC neutrino beam

The J-PARC main ring provides a 30 GeV proton beam which collides with a graphite target to produce secondary hadrons such as pions and kaons. The secondary hadrons are focused by magnetic horns and subsequently decay in a 96 m decay volume to produce an intense neutrino beam, e.g. $\pi \rightarrow \mu + \nu_\mu$. The polarity of the horn current determines whether positive or negative meson are focused, which in turn determines whether the neutrino beam is largely composed of muon neutrino or muon anti-neutrino.

Table 1.1: Summary of the systematic uncertainties on the predicted rate of ν_μ CC and ν_e CC candidate events with constraint from ND280 measurement [13].

Source of uncertainty	ν_μ CC	ν_e CC
Flux and common cross sections	2.7%	3.2%
Cross sections due to the difference of the target material between water and hydrocarbon	5.0%	4.7%
SK detector	4.0%	2.7%
Final or secondary hadronic interaction	3.0%	2.5%
Total	7.7%	6.8%

The T2K experiment employs the off-axis method to generate a narrow-band neutrino beam due to the kinematics of mesons decay. In this method the neutrino beam is purposely directed at an angle with respect to the baseline connecting the proton target and the SK detector. The off-axis angle of the SK detector is set at 2.5 degrees to produce a 600 MeV neutrino flux, which maximizes muon neutrino oscillation probabilities at the 295 km baseline.

1.2.2 Detectors

The near detector site at 280 m downstream of the production target houses the on-axis and off-axis detectors. The on-axis detector, INGRID (Interactive Neutrino GRID), measures the neutrino beam direction and profile. The off-axis detector, ND280, measures the neutrino flux, energy spectrum, and cross sections in order to characterize signal and background events that are observed in the far detector. ND280 mainly detects forward scattering muons produced by neutrino interaction on hydrocarbon.

The far detector, Super-Kamiokande, is a 50 kton water Cherenkov detector located in the Kamioka Observatory. The detector contains approximately 13,000 photomultiplier tubes (PMTs) that image neutrino interaction on water. The 20-inch PMTs cover inside the water tank with 4π angular acceptance.

1.2.3 Current status and future prospects

The T2K experiment has observed the ν_e appearance with more than 7.3σ significance and measured the mixing angle $\sin^2 2\theta_{13} = 0.140_{-0.032}^{+0.038}$ ($0.170_{-0.037}^{+0.045}$) assuming normal (inverted) hierarchy [14]. In addition, the mixing angle $\sin^2 \theta_{23} = 0.514_{-0.056}^{+0.055}$ (0.511 ± 0.055) is obtained by the measurement of ν_μ disappearance. The part of the region of the CP phase $\delta_{CP} = [0.15, 0.83]\pi$ ($[-0.08, 1.09]\pi$) is excluded at 90% confidence level by combining the result of T2K and the reactor experiments [13].

T2K aims for the more precise measurement of the neutrino oscillation. It is important to reduce not only the statistical uncertainty but also the systematic uncertainty. Table 1.1 summarizes the systematic uncertainties on the predicted rate of charged current (CC) events. The use of different target materials between the SK detector and ND280 causes the largest systematic uncertainty in both of ν_μ and ν_e CC events. Moreover, the difference of the angular acceptance between the SK detector and ND280 also contributes to the systematic uncertainty.

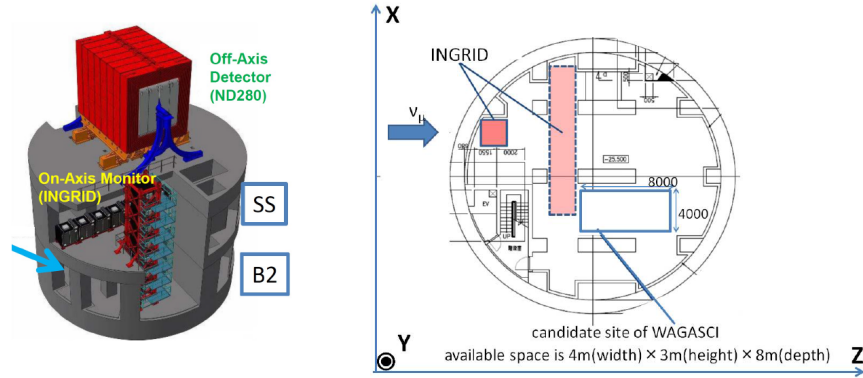


Figure 1.2: A candidate site of the WAGASCI detector. The left figure shows the neutrino monitor hall at J-PARC, where ND280 and INGRID are located. The right figure is a top view of the B2 floor [16].

The reduction of these systematic uncertainties leads to the further precise measurement of the neutrino oscillation.

1.3 WAGASCI experiment

1.3.1 Motivation

In order to reduce the uncertainties of neutrino cross section due to the difference of the target material in T2K, we have been developing a new neutrino detector named WAGASCI (Water Grid And SCIntillator detector). The WAGASCI detector contains targets made of water (H_2O) and hydrocarbon (CH) to measure neutrino cross section on both materials. The WAGASCI experiment aims to measure the charged current cross section ratio between H_2O and CH with 3% accuracy by using the J-PARC neutrino beam [15, 16]. The uncertainty of neutrino flux leads to the large uncertainty in the measurement of absolute cross section. Taking the ratio of cross sections by using the same neutrino flux, however, the flux uncertainty could be canceled and the precise measurement would be achieved [17].

1.3.2 Location of the detector

The WAGASCI detector will be installed at the B2 floor of the neutrino monitor hall in J-PARC. Figure 1.2 shows a candidate site of the WAGASCI detector. The location of the detector will be at 1.6 degrees off-axis, where the neutrino energy spectrum is similar to that in T2K, at 2.5 degrees off-axis. Figure 1.3 shows the expected neutrino energy spectrum that peaks at around 600 MeV.

1.3.3 Detector design

The WAGASCI detector consists of two parts, a central detector and surrounding muon range detectors (MRDs) as shown in Fig. 1.4. The central detector is a neutrino interaction target made

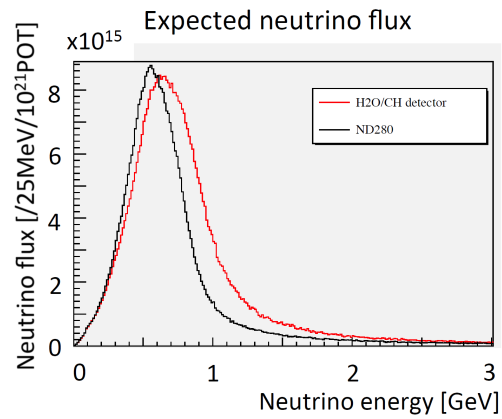


Figure 1.3: The expected neutrino energy spectrum at the candidate site of the WAGASCI detector (red line) and at the site of ND280 (black line) [16].

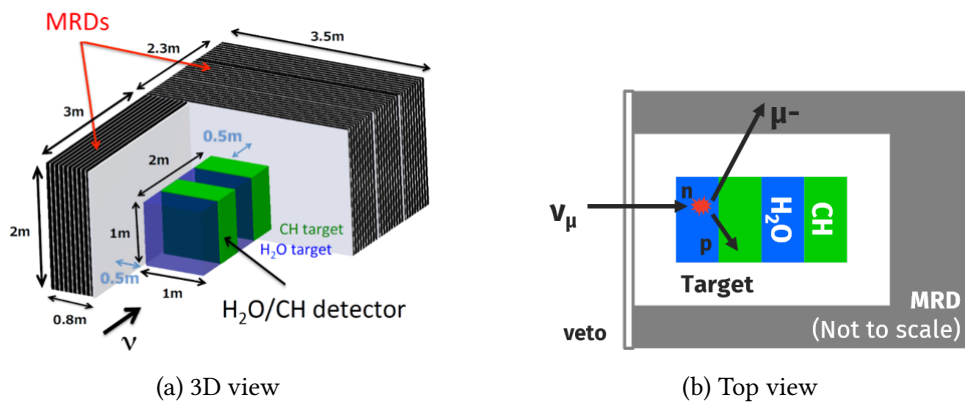


Figure 1.4: The configuration of WAGASCI detector.

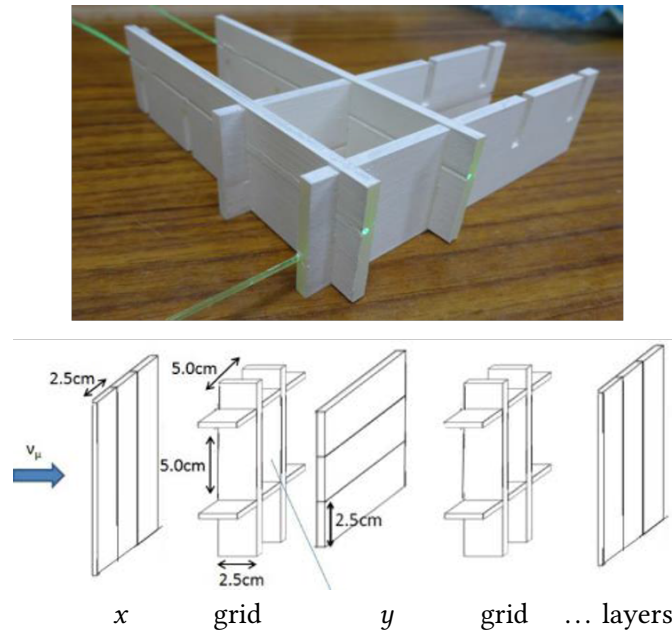


Figure 1.5: The 3D grid-like structure of the 3-mm thick scintillators.

of H_2O and CH. The mass of the H_2O and CH targets is 1 ton each, and the outer dimension of the central detector is $1 \times 1 \times 2 \text{ m}^3$. The H_2O and CH targets are arranged in alternating sequence along the beam axis in order to reduce the difference of the neutrino flux and the acceptance of MRDs in each target material, because these difference causes systematic uncertainty in the measurement of cross sections.

The central detector also contains 3-mm thick scintillators assembled into a 3D grid-like structure as shown in Fig. 1.5. The size of the scintillator is $1000 \times 25 \times 3 \text{ mm}^3$. The grid-like structure are composed of several layers and arranged in the order of x layer, grid layer, y layer, and grid layer. Scintillators that have slits in every 50 mm are assembled into a grid layer as the slits cross each other. When neutrinos interact with the target, charged particles are produced and detected by scintillators. This structure enables us to reconstruct the track of charged particles produced by neutrino interaction in the target with a large angular acceptance. The empty space enclosed by the scintillators is $50 \times 50 \times 25 \text{ mm}^3$ and filled with the neutrino target materials, H_2O or CH.

The scintillation light is collected by a wavelength shifting (WLS) fiber (Y-11(200), Kuraray) that is coupled to a Multi-Pixel Photon Counter (MPPC) from Hamamatsu. The WLS fibers are used to reduce the attenuation of the scintillation light. Neutrino interactions on scintillators in the water target causes background events because they are not distinguishable from signal events of neutrino interactions on water. The thin scintillators are used in order to maximize the ratio of water mass to total mass in a fiducial volume up to 79%. In order to obtain sufficient light yield, newly developed MPPCs with low optical crosstalk and high photon detection efficiency (PDE) will be used in the central target.

The MRDs are located on the left side, the right side, and downstream of the central target. They consist of 3 or 6-cm thick iron plates and 7-mm thick scintillators. The scintillation light

is collected by a WLS fiber that is coupled to a MPPC as with the central detector. The MRDs measure the momentum of muons produced by charged current interaction up to 1 GeV/c. A magnetic option for the downstream MRD, Baby-MIND, is considered to distinguish negative sign muon produced by neutrinos and positive sign muon produced by anti-neutrinos [18, 19].

The WAGASCI detector will have a large number of readout channels. The total number of channels will be about 8000. It is important to measure the basic characteristics of MPPCs before installation in the detector. A characterization system to measure a large number of MPPCs has been developed.

1.4 Contents of this thesis

This thesis reports the characterization of MPPCs for the WAGASCI detector. Chapter 2 introduces an operation principle and features of MPPC. Recent development and characteristic measurement of new MPPCs are presented in Chapter 3. Chapter 4 describes the development of characterization system for the large number of MPPC. Finally, future prospects and summary are presented in Chapter 5.

Chapter 2

Multi-Pixel Photon Counters

The Multi-Pixel Photon Counter (MPPC), developed by Hamamatsu, is one of the devices called silicon photomultipliers (SiPM). It is a photon-counting device using multiple avalanche photodiode (APD) pixels operating in the Geiger mode [20]. The MPPC features high gain and high photon detection efficiency (PDE), while it has false signals such as dark noise, afterpulse, and optical crosstalk. In this chapter, an operation principle and features of APD, SiPM, and MPPC are presented.

2.1 Avalanche Photodiode

The APD is a highly sensitive photodiode using avalanche multiplication. It is one of the semiconductor photon detectors that exploits photoelectric effect to convert light into current. By applying a reverse bias voltage, the APD operates at high speed and features high gain, high sensitivity, and higher S/N than PIN photodiodes.

2.1.1 Principle of avalanche multiplication

A photodiode has a PN junction or PIN structure. The intrinsic region at the junction between the P-layer and N-layer is known as the depletion layer. When a photon of higher energy than the band gap energy strikes the photodiode, the valence band electrons are excited to the conduction band, leaving holes in their place in the valence band as shown in Fig 2.1. In the depletion layer the electric field accelerates these electron-hole pairs in the opposite directions and generates a photocurrent. These electrons and holes generating a current flow in a semiconductor are called the carriers. A normal photodiode does not multiply photocurrent. When one photon is absorbed, only one electron-hole pair is created and small photocurrent is extracted. Therefore it is difficult for the normal photodiode to detect a weak light.

The APD has the same mechanism of photocurrent generation as that of a normal photodiode. A reverse bias voltage applied to the APD creates the electric field across the PN junction. The higher the electric field strength, the higher the drift speed of these accelerated carriers. When the electric field reaches a certain level, however, the carriers are more likely to collide with the crystal lattice and create new electron-hole pairs. These electron-hole pairs then create additional electron-hole pairs, which generate a chain reaction of ionization that is called

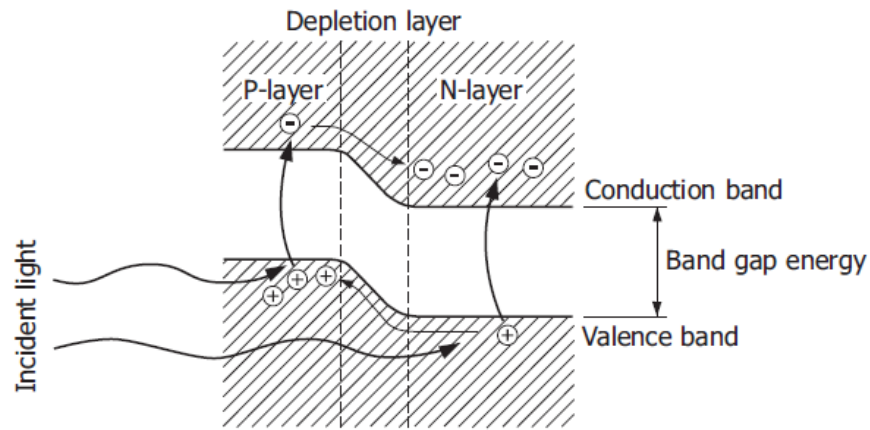


Figure 2.1: PN junction state of photodiodes [21].

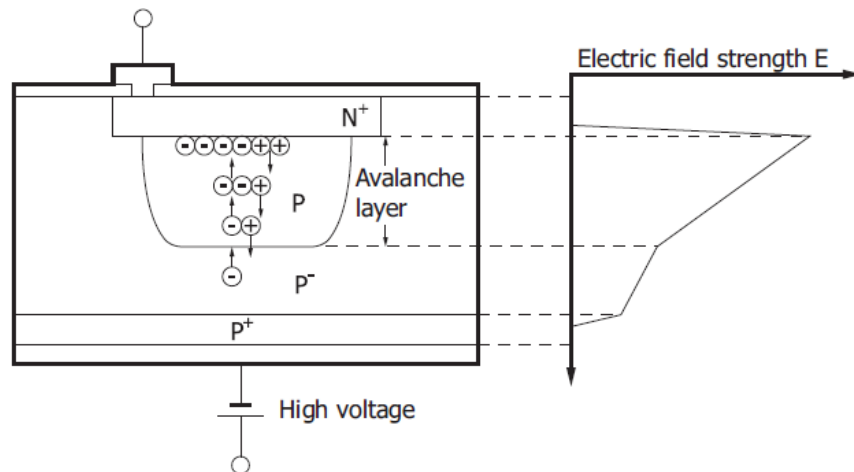


Figure 2.2: Schematic diagram of avalanche multiplication [21].

Table 2.1: The characteristics of the APD operating in normal mode and Geiger mode.

	Normal mode	Geiger mode
Operation voltage	Lower than the breakdown	Higher than the breakdown
Gain	10 ~ 100	$10^5 \sim 10^6$
Photocurrent	In proportion to the number of detected photons	Independent on the number of detected photons

avalanche multiplication. The number of carriers increases in a geometrical progression when the carriers move through the avalanche layer as shown in Fig 2.2.

2.1.2 Geiger mode

The gain of APD strongly depends on the electric field across the depletion layer. In the normal operation range that is called normal mode, the gain increases as applied bias voltage increases, and the photocurrent increases as the number of detected photons increases. The gain is 10 ~ 100, thus it is difficult to detect one photon signal. As the bias voltage is increased more, however, the APD eventually reaches the breakdown voltage and operates in the Geiger mode. The gain of about 10^6 is achieved, and the photocurrent is saturated to be independent on the number of detected photons. The characteristics of the APD operating in normal mode and Geiger mode is summarized in Table 2.1.

The number of electron-hole pairs generated during the time that a carriers moves a unit distance is referred to as the ionization rate. These ionization rate are important factors in determining the multiplication mechanism. Because the ionization rate of electron in silicon is larger than that of holes, accelerated electrons mainly cause the avalanche multiplication in normal mode. The avalanche multiplication stops when all electrons move outside of the avalanche layer. Yet in the Geiger mode, holes also create electron-hole pairs and cause the avalanche multiplication. Both of electrons and holes cause the avalanche multiplication again and again, therefore high gain is achieved.

The APD operating in the Geiger mode generates a large output by the discharge even when detecting a single photon. Once the Geiger discharge begins, it continues as long as the electric field in the APD is maintained. In order to halt the Geiger discharge and detect the next photon, a quenching resistor is usually connected in series with the APD. Figure 2.3 shows the basic operation process of a combination of the APD operating in the Geiger mode and the quenching resistor. When the APD with the bias voltage applied at the operation voltage (V_{op}) detects photons, the Geiger discharge begins and generates a current. The quenching resistor reduces the operating voltage of the APD when the Geiger discharge flows in the resistor. The operating voltage decreases to the breakdown voltage (V_{br}), then the avalanche multiplication calms down. When the current stops, the APD begins to charge again and becomes to be able to detect the next photon. Output signal of the APD shapes a pulse that rises as the Geiger discharge and falls as quenching.

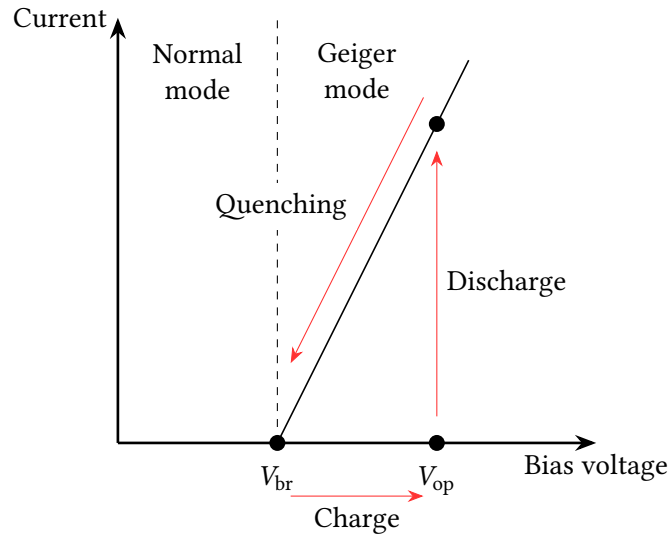


Figure 2.3: The basic operation process of a combination of the APD operating in the Geiger mode and the quenching resistor.

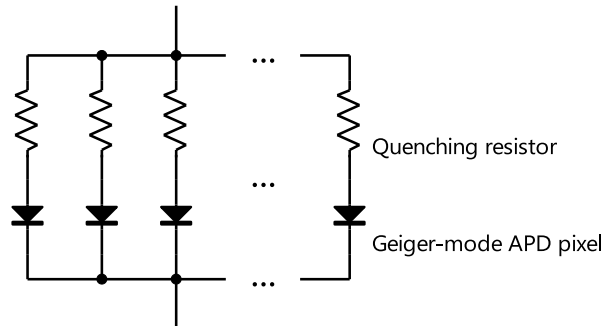


Figure 2.4: Structure of the SiPM.

2.2 Silicon Photomultiplier

The APD operating in the Geiger mode generates a saturated photocurrent independent on the number of detected photons while it features high gain. It cannot provide proportional information regarding the intensity of incident photons. Therefore, a silicon-based photomultiplier called SiPM is developed to have capability to count the number of detected photons by using multiple APD pixels operating in the Geiger mode. The SiPM is also called Pixelated Photon Detector.

Figure 2.4 shows a structure of the SiPM. One pixel of the SiPM is a combination of the APD operating in Geiger mode and the quenching resistor. A large number of pixels are connected in parallel and arranged in two dimensions. Each pixel in the SiPM generates a pulse at the same amplitude when it detects a photon. The pulses generated in multiple pixels are read out in the superposition. For example, when three photons are injected to different pixels and

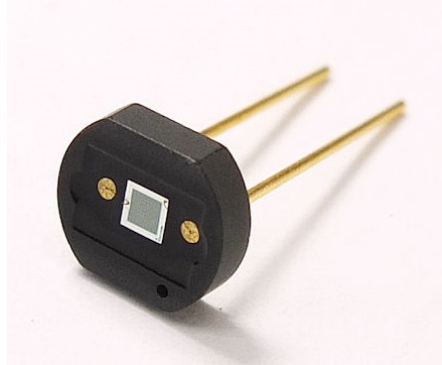


Figure 2.5: Picture of ceramic packaged MPPC.

detected at the same time, the SiPM generates a signal with three times amplitude as the SiPM detects one photon. The SiPM is able to count the number of detected photons by measuring amplitude of output signal or amount of generated charge.

2.3 Characteristics of MPPC

While various SiPMs have been developed around the world and used for a lot of applications, we focus on the MPPC developed by Hamamatsu, in Japan. Figure 2.5 shows the conventional ceramic packaged MPPC. The MPPC operates on a low voltage of around 50 V and features a high gain, high PDE, fast response, good time resolution, and wide spectral response range. These features provide the high performance for photon counting. The MPPC is also immune to magnetic fields and highly resistant to mechanical shocks, which are advantages unique to solid-state devices.

The MPPC is able to count the number of detected photon by measuring output signal. When the MPPC detects n photons, the output is called n photon equivalent (p.e.) signal.

2.3.1 Gain

The gain of the MPPC is defined as the output charge when one pixel detects a photon, divided by the elementary charge. Let M , Q , and $e = 1.602 \times 10^{-19}$ C be the gain, the output charge of the MPPC, and the elementary charge, respectively. The gain is expressed as

$$M = \frac{Q}{e}. \quad (2.1)$$

The output charge depends on the operation voltage (V_{op}) and breakdown voltage (V_{br}) as

$$\begin{aligned} Q &= C(V_{op} - V_{br}) \\ &= CV_{over}, \end{aligned} \quad (2.2)$$

where C is capacitance of one pixel, and $V_{over} = V_{op} - V_{br}$ is called the over voltage. The gain has good linearity to the over voltage. The PDE, dark noise, and so on also increase as the applied over voltage increases. The over voltage dependence of each characteristics is important in application of the MPPC.

The temperature dependence of the breakdown voltage has an effect on the gain when the constant operation voltage is applied. As the temperature rises, the crystal lattice vibrations become stronger. These vibration in lattice obstruct the carriers and decreases the probability of ionization. The high operation voltage is needed to make the MPPC reach the breakdown at high temperature. The temperature dependence of the breakdown voltage is typically 60 mV/degree.

2.3.2 Photon detection efficiency

The PDE is defined as the ratio of the number of detected photons to the number of incident photons. The PDE is expressed by the product of a geometrical fill factor, quantum efficiency (QE), and avalanche probability as

$$\text{PDE} = \text{Fill factor} \times \text{QE} \times \text{Avalanche probability}. \quad (2.3)$$

The geometrical fill factor is the ratio of the effective photosensitive area to the total photosensitive area. It is around 60% for the MPPC whose pixel pitch is 50 μm , which is used in the T2K experiment and WAGASCI experiment. The quantum efficiency is the ratio of the number of generated electron-hole pairs to the number of detected photons. It depends on the wavelength of detected photons. The avalanche probability is the probability that carriers cause ionization in avalanche layer. The PDE increases as applied over voltage increases due to the over voltage dependence of the avalanche probability.

2.3.3 Dark noise

The MPPC produce pulses not only by incident photons but also by thermal excitation. The pulses produced by the thermal excitation are called the dark noise. The dark noise is not distinguishable from the signal produced by incident photons because the dark noise is also multiplied to a 1 p.e. signal level. The dark noise rate can be measured by counting the number of output signals that exceed a threshold of 0.5 p.e. signal level, without incident photons.

The dark noise rate increases in proportion to the photosensitive area, as the applied over voltage increases, and as the temperature rises. The temperature dependence of the dark noise rate is expressed as

$$\text{Dark noise rate} \propto T^{\frac{3}{2}} \exp\left(\frac{E_g}{2k_B T}\right), \quad (2.4)$$

where T , k_B , and E_g are the absolute temperature, Boltzmann's constant, and band gap energy of silicon, respectively.

2.3.4 Optical crosstalk

The avalanche multiplication occurring by either a detected photon or a thermal excitation in one pixel may emit secondary photons due to bremsstrahlung or recombination. When a secondary photon is detected by other pixels, Geiger discharge also occur in this pixel. This process is called optical crosstalk, and its probability increases as the over voltage increases. It takes less than 1 ns that a secondary photon is emitted from one pixel and detected by the other pixels. The pulse output from the pixel that detects a secondary photon is not distinguishable

from the pulse output from the pixel that emits a secondary photon. The optical crosstalk affects pulse linearity, dynamic range, and photon counting resolution.

2.3.5 Afterpulse

In the avalanche multiplication a carrier may be trapped by lattice defect temporary and released from a few ns to hundreds ns after to cause the avalanche multiplication again. The pulse caused by trapped carrier is called afterpulse, and its probability increases as the over voltage increases. Because the output signal of MPPCs in the application is shaped or integrated in certain time window, the afterpulse occurring in the time window makes the signal be larger than the original. The afterpulse also affects pulse linearity, dynamic range, and photon counting resolution.

Chapter 3

Development of MPPC

3.1 History of MPPC development

The first generation MPPC, the S10362 type by Hamamatsu, was released in 2006 as a newly developed semiconductor photosensor [22]. The T2K experiment has been using around 56000 first generation MPPCs in their near detectors since 2009 [23]. Since then, the performance of MPPC has been significantly improved. Various MPPCs have been developed and used for a lot of applications in a wide range of fields. Some have large photosensitive area and others have UV-sensitivity.

In this study, we focus on new MPPCs that are successors to the S10362 type with low dark noise, low optical crosstalk, and high PDE. The afterpulse and dark noise suppression type (S12825) was released in summer 2013. Then, the optical crosstalk suppression type (S13081) was released in winter 2014. Table 3.1 summarizes some features of these three types of MPPCs, which we measured in this study. Each device is ceramic packaged type and single channel MPPC. The pixel size is $50 \times 50 \mu\text{m}^2$ for all types. The newest MPPC, S13081 type, will be used for the WAGASCI detector.

3.2 Performance of MPPC

The characteristics of new MPPCs are measured in comparison with the first generation MPPC. One device of each MPPC in Table 3.1 is measured in this study. Figure 3.1 shows a readout circuit used for performance test of MPPCs. A reverse bias voltage is applied to the measured MPPC by using a DC power supply. An output is amplified and connected to an oscilloscope,

Table 3.1: Three types of MPPC measured in this study. The size of pixel is $50 \mu\text{m}$ for all types.

Type number	Features	Number of pixels	Photosensitive area
S10362-11-050C	First generation MPPC ¹	400	$1 \times 1 \text{ mm}^2$
S12825-050C	Afterpulse suppression	667	$1.3 \times 1.3 \text{ mm}^2$
S13081-050CS(X1)	Crosstalk suppression	667	$1.3 \times 1.3 \text{ mm}^2$

¹It is same type as used in T2K near detectors (S10362-13-050C) but has different photosensitive area.

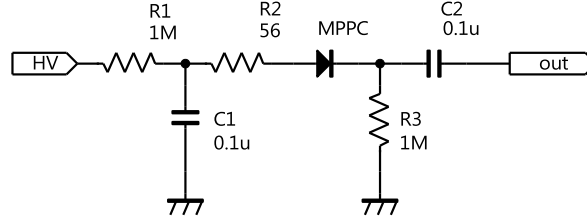


Figure 3.1: Readout circuit used for performance test of MPPCs.

a discriminator, or an ADC. The following characteristics of MPPCs are measured; dark noise rate, optical crosstalk, gain, and relative PDE. The measurements are carried out at 20°C.

Figure 3.2 shows the waveforms of the MPPCs measured with an oscilloscope. These waveforms are due to dark noise of MPPCs with 2.0 V over voltage applied. Waveforms corresponding to 1 p.e. pulse, 2 p.e. pulse, and so on can be clearly identified. More than 2 p.e. pulses in the dark noise are assumed to be caused by optical crosstalk. The waveform of the S12825 type MPPC shows a significant decrease of afterpulsing compared with the S10362 type MPPC. The waveform of the S13081 type MPPC shows a significant decrease of optical crosstalk compared with the earlier devices. Figure 3.3 shows micrographs of the MPPC pixel. A trench to prevent crosstalk features the S13081 type MPPC, while the S10362 type and S12825 type MPPC look similar.

3.2.1 Dark noise rate

Figure 3.4 shows the diagram of setup for measuring dark noise rate and optical crosstalk. No light source is used in this measurement. The dark noise rate is measured by counting the rate of discriminated signals with a 0.5 p.e. threshold level. The threshold voltage is determined by measuring the voltage of pulse height corresponding to 1 p.e. signal with the oscilloscope. The dark noise rates normalized to 1 mm² active area are shown as a function of applied over voltage in Fig. 3.5a. The S12825 type and the S13081 type MPPCs have an order of magnitude lower dark noise rate than the S10362 type MPPC. The significant decrease of the dark noise enables us to operate the new MPPCs with higher over voltage.

3.2.2 Optical crosstalk

The optical crosstalk probability is calculated as the ratio of the rate of discriminated signals with 0.5 p.e. and 1.5 p.e. threshold level:

$$\text{Optical crosstalk probability} = \frac{\text{The rate of dark noise over 1.5 p.e. threshold}}{\text{The rate of dark noise over 0.5 p.e. threshold}}. \quad (3.1)$$

Figure 3.5b shows the measured optical crosstalk. Compared to the S10362 type MPPC, the S13081 type MPPC has one tenth optical crosstalk, while the S12825 type MPPC has slightly higher optical crosstalk. The substantial suppression of optical crosstalk enables us to lower the signal threshold level in our application.

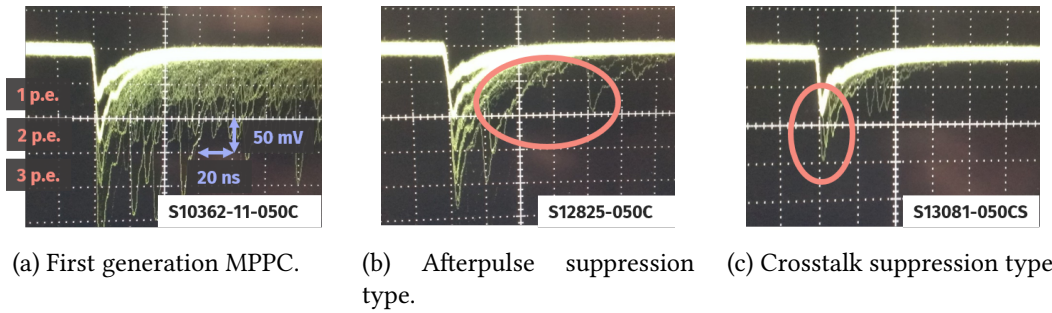


Figure 3.2: The waveforms of the three different MPPCs. Compared with figure (a) afterpulsing is decreased in figure (b), and compared with figure (a) and (b) optical crosstalk is decreased in figure (c).

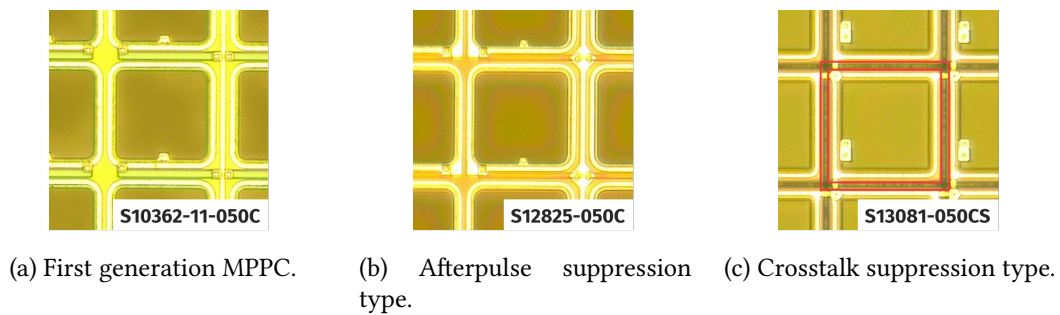


Figure 3.3: The micrographs of MPPCs. There is a trench to prevent crosstalk in the S13081 type MPPC (red box).

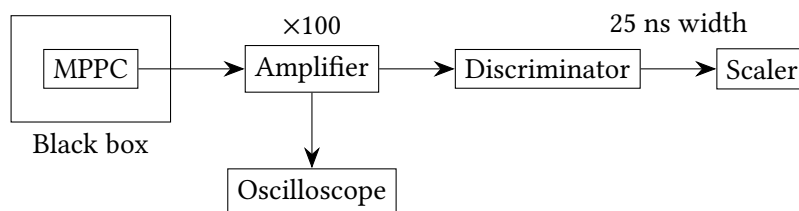


Figure 3.4: The diagram of setup for measuring dark noise rate and optical crosstalk.

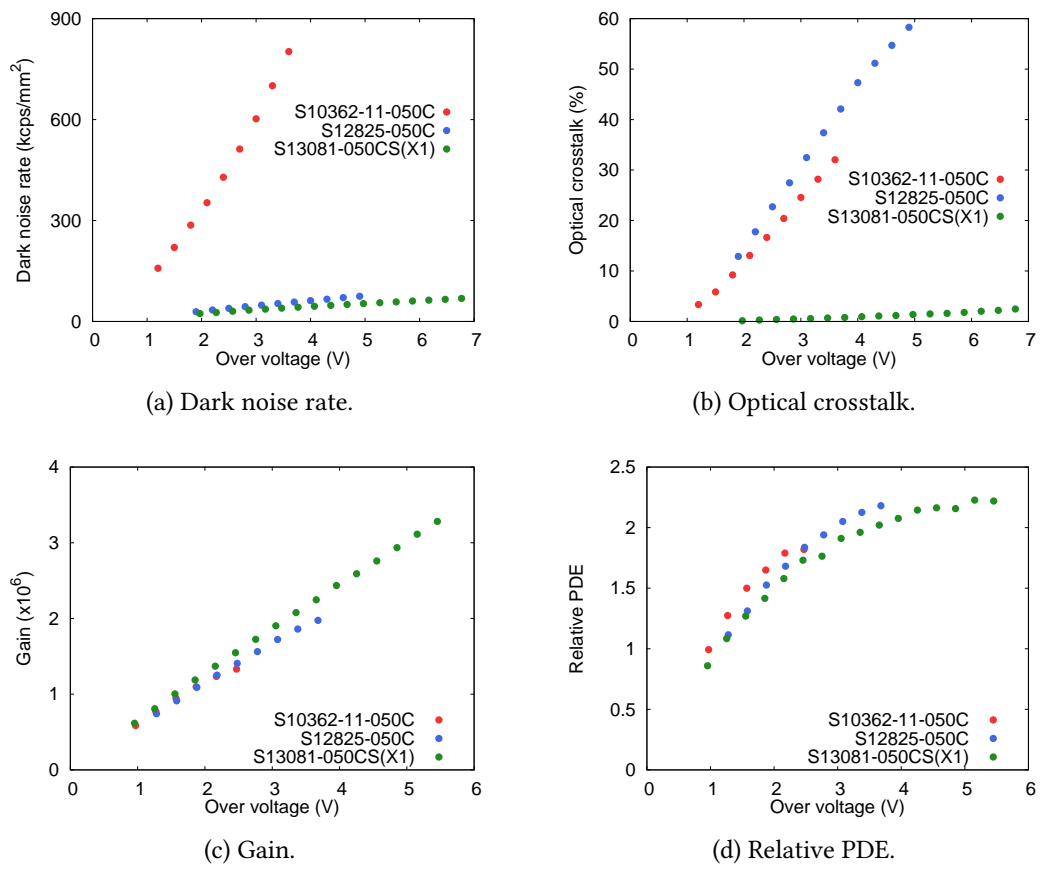


Figure 3.5: The results of the performance test for each MPPCs.

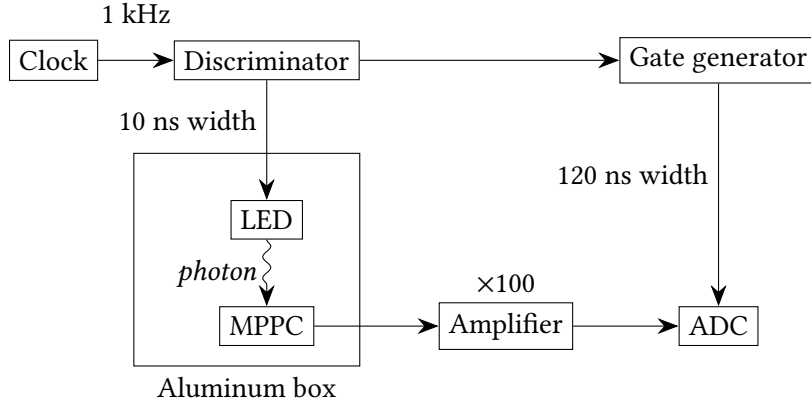


Figure 3.6: The diagram of setup for measuring gain and relative PDE.

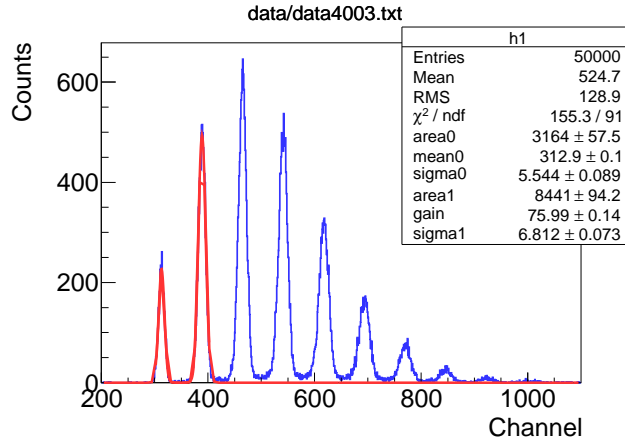


Figure 3.7: A typical charge distribution of MPPC. Blue line shows measured charge distribution of MPPC and red line shows fitted Gaussian functions. The most left peak corresponds to pedestal events and the right peak next to pedestal corresponds to 1 p.e. events.

3.2.3 Gain

Figure 3.6 shows the diagram of setup for measuring gain and relative PDE. Light emitted from an LED with a wavelength of 470 nm is injected to the MPPCs because WLS fibers used in our application emits light with spectrum peak around 470 nm. A piece of white paper is used to cover the LED and diffuse emitted light uniformly. The MPPC signals are amplified and recorded with a charge integrating ADC. A 1 kHz clock signal is used to flash the LED and to generate a 120-ns wide ADC gate. A typical charge distribution of MPPC is shown in Fig. 3.7. Peaks corresponding to 0 p.e. (pedestal) events, 1 p.e. events and so on can be clearly identified and are fitted with a sum of two Gaussian functions. The gain is calculated from the difference of ADC counts between pedestal events and 1 p.e. level events as

$$\text{Gain} = (\text{ADC counts of 1 p.e. events}) - (\text{ADC counts of pedestal events}). \quad (3.2)$$

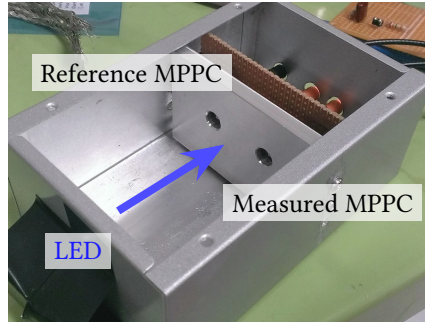


Figure 3.8: A picture of setup for measuring relative PDE.

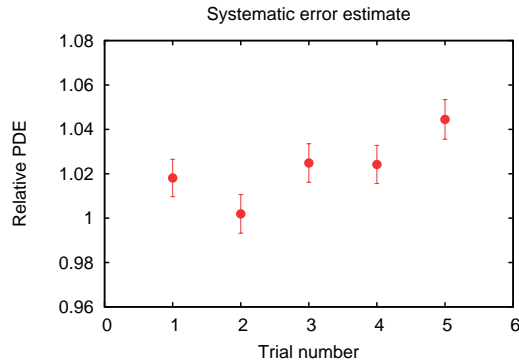


Figure 3.9: Variation of measured relative PDE due to MPPC replacement.

Figure 3.5c shows the measured gain. The gain of each MPPC is the same order of magnitude for the same over voltage, but the newer MPPCs can be operated over a wider range of operation voltages. With higher over voltage applied, the new MPPC can achieve higher gain and is relatively immune to temperature changes.

3.2.4 Relative PDE

When measuring the relative PDE, two MPPCs are measured at the same time in order to reduce the uncertainty of light intensity of LED. One is a measured MPPC and the other is a reference MPPC as shown in Fig. 3.8. The S10362 type MPPC is used as the reference in this study. The relative PDE is calculated as the ratio of the number of photons detected by each MPPCs to the number of photons detected by the reference MPPC with 1.0 V over voltage:

$$\text{Relative PDE} = \frac{\text{Number of photons detected by each MPPC}}{\text{Number of photons detected by the reference MPPC with 1.0 V over voltage}}. \quad (3.3)$$

The number of photons detected by the MPPC is calculated as $-\ln(P_0)$, where P_0 is the fraction of events in which no photon is detected. This method is commonly applied when measuring MPPCs and avoids a bias due to afterpulse and optical crosstalk because afterpulse and optical crosstalk only affect the number of events in which one or more photons are detected. Let P_n be probability that n photons are detected by the MPPC. Assuming the true

Table 3.2: The comparison of the performance of MPPC. The values are normalized by that of the S10362 type MPPC.

Type number	Applied over voltage	Dark noise rate	Optical crosstalk	Gain	Relative PDE
S10362-11-050C	1.1 V ²	1	1	1	1
S13081-050CS(X1)	1.1 V	0.077	<0.03	1.1	0.87
S13081-050CS(X1)	4.0 V	0.25	0.21	3.6	1.9

number of detected photons follow the Poisson distribution, P_n is represented as

$$P_n = \frac{\lambda^n e^{-\lambda}}{n!}, \quad (3.4)$$

where λ is the mean of the number of detected photons. Then, λ can be calculated by using P_0 as

$$P_0 = e^{-\lambda}, \quad (3.5)$$

$$\therefore \lambda = -\ln(P_0). \quad (3.6)$$

An effect of dark noise is subtracted from λ , which is calculated by using measured dark noise rate for each MPPC and width of ADC gate signal. The effect of dark noise is typically evaluated as about 0.06 in units of the number of detected photons by using the gate width of 120 ns and the typical dark noise rate of 50 kHz for the optical crosstalk suppression type.

Attaching and detaching MPPCs to change the measured device may cause the uncertainty in the measurement of the relative PDE. A systematic error due to replacing MPPCs is estimated by measuring the relative PDE of the same MPPC five times, attaching and detaching MPPCs in every measurement. Figure 3.9 show the result of five measurements. The systematic error of measuring the relative PDE is assumed to be about 3%, that is deviation of the relative PDE in these measurements. Finally, the relative PDE of each MPPC is shown in the Fig. 3.5d. The newer MPPCs have slightly lower PDE than the S10362 type MPPC for the same over voltage. With higher over voltage applied, however, the newer MPPCs can achieve higher PDE.

3.2.5 Summary

The performance of the MPPC is summarized in Table 3.2. The new MPPC can achieve ten times lower dark noise rate, more than ten times lower optical crosstalk, higher gain, and higher PDE when higher over voltage is applied. Therefore, the MPPCs used in the WAGASCI detector will be operated with about 4.0 V over voltage.

²The value of 1.1 V over voltage is used in the INGRID, one of the T2K near detectors, to operate MPPCs.

Chapter 4

Development of MPPC characterization system

The WAGASCI detector will have a large number of readout channels. A characterization system to measure a large number of MPPCs has been developed. The gain, relative PDE, dark noise rate, and optical crosstalk will be measured for different temperature and over voltage.

4.1 Requirements

4.1.1 Outline

The process of measurement will be automated to reduce the burden and mistakes. The measurements are carried out at 15, 20, and 25°C in a temperature controlled chamber. These temperatures are determined because the temperature of the neutrino monitor hall is around 20°C. The gain and relative PDE are measured with a light source, while the dark noise rate and optical crosstalk are measured without a light source. It is required that the characterization system is able to monitor light intensity by each measurements and to switch the light source on and off.

4.1.2 MPPCs used for the WAGASCI detector

In order to realize a compact readout with a large number of channels, we developed an array of MPPCs for the central target of the WAGASCI detector as shown in Fig. 4.1. The array consists of 32 MPPCs that are crosstalk suppression type. Each MPPC has 1.5 mm diameter photosensitive area and 716 pixels of $50 \times 50 \mu\text{m}^2$ pixel size. The signals of MPPC are read out via flexible printed circuit (FPC) cables. The array of MPPCs will be used in the central target, while the single channel MPPCs will be used in the MRDs. The total number of channels used in the WAGASCI detector will be 8126 including 5376 in the arrays of MPPCs and 2750 in the single channel MPPCs. It is required that the characterization system enables us to measure both of the array of MPPCs and single channel MPPC; a large number of channel of MPPC simultaneously; and automatically as far as possible.

Two types of MPPC arrays will be measured. One is a common cathode array (S10943-4156(X)) that has common cathode for each 16 channels. The other is a independent cathode

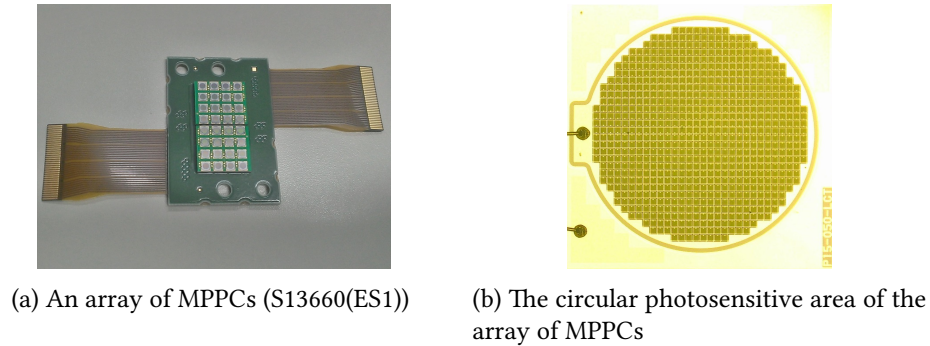


Figure 4.1: An array of MPPCs.

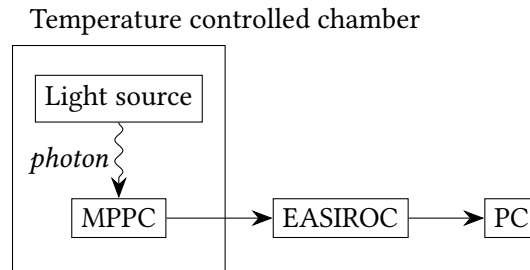


Figure 4.2: The basic concept of characterization system.

array (S13660(ES1)) that has independent cathode channel by channel. A type number of single channel MPPC is S13081-050CS(X1), which is the conventional ceramic packaged type and crosstalk suppression type as mentioned in section 3.2.

4.2 Design of the characterization system

Figure 4.2 shows the basic concept of characterization system. MPPCs and a light source are placed in a temperature controlled chamber. Photons are emitted from the light source and detected by the MPPCs. The signals from the MPPCs are read out by using NIM EASIROC module controlled via a PC.

4.2.1 NIM EASIROC module

NIM EASIROC module is general purpose MPPC readout module [24] as shown in Fig 4.3. A front-end ASIC named Extended Analogue SiPM Read Out Chip (EASIROC) developed by Omega/IN2P3 in France is used in this module. An EASIROC chip has 32 MPPC inputs and all essential functions to operate many MPPCs such as amplifier, discriminator, and bias voltage adjustment. Figure 4.4 shows a schematic of one channel in EASIROC chip. The bias voltage applied to each MPPC channels is individually adjustable up to 4.5 V by using 8-bit input DAC. An EASIROC chip has two amplifiers with high and low gain with a factor 10 of gain difference. The amplified signals are shaped by the slow and fast shapers. The pulse height of the slow shaper output is stored to the analogue buffer by using a sample and hold circuit. The external



Figure 4.3: Picture of NIM EASIROC module.

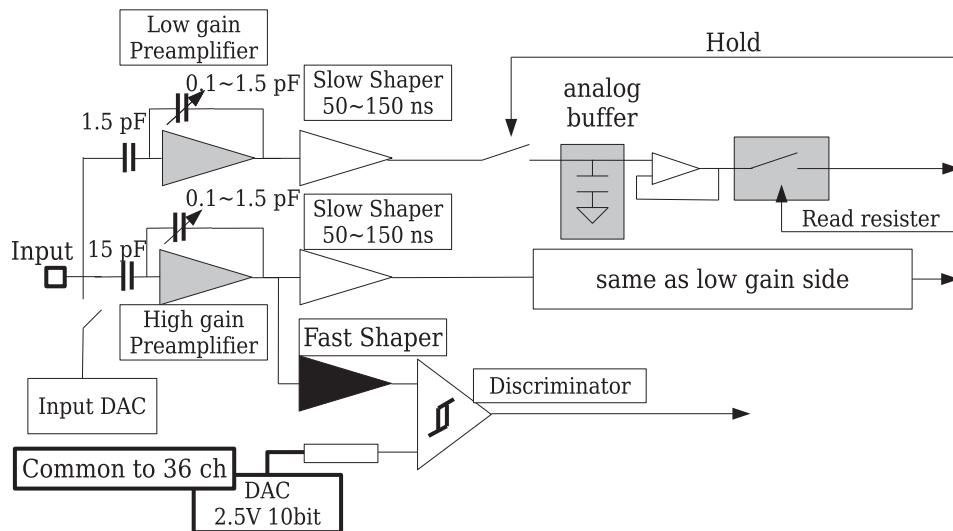


Figure 4.4: A schematic of one channel in EASIROC chip [24].

Table 4.1: Digital inputs and outputs of NIM EASIROC module

Type	Name	Note
Input	HOLD	Determine the timing of holding the shaper output
	T STOP	Reset the counts of scaler, 100 ns after HOLD signal
	ACCEPT	Send the data to PC, 4 μ s after HOLD signal
Output	SYNC OUT	Output clock signal



Figure 4.5: Temperature controlled chamber.

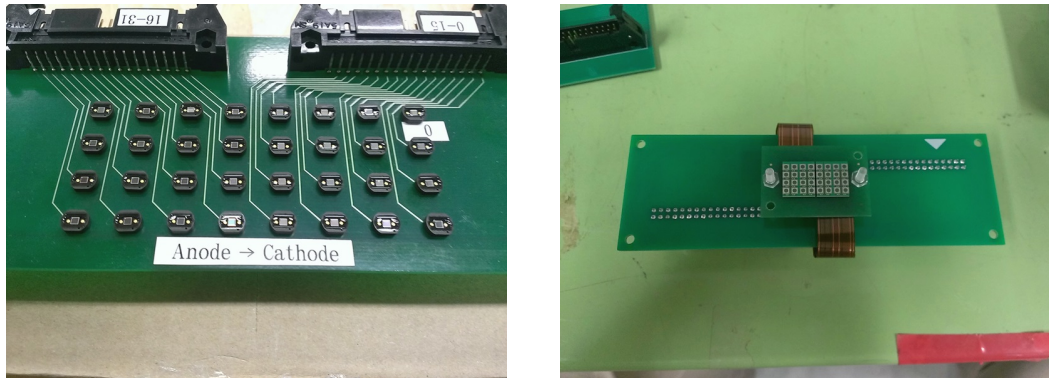
hold signal of NIM level determines the timing of sampling the voltage. The stored voltage is read via the read register serially in readout period. The discriminated signal from fast shaper is read out individually. The bias voltage, the voltage of input DAC, the gain of amplifiers, the shaping time of shapers, and the threshold voltage of discriminator are controllable via text files.

Two EASIROC chips, an FPGA, two ADCs, and a bias voltage supplier are used in a module. The FPGA controls the configuration of EASIROC and data acquisition by using an ADC, TDC, and scaler. An adjustable bias voltage of 0–90 V is commonly supplied to all MPPC channels.

A NIM EASIROC module has several inputs and outputs of NIM level signal. Table 4.1 summarizes these inputs and outputs that are used in the characterization system. Three inputs, HOLD, T STOP, and ACCEPT, determine the timing of readout sequence such as sampling the voltage. The output named SYNC OUT controlled by FPGA outputs 0/1 NIM logic signal or a square wave of the specified frequency. We will use the 0/1 NIM logic signal to synchronize multiple EASIROC modules or to switch the light source on and off.

4.2.2 Temperature controlled chamber

Figure 4.5 shows the temperature controlled chamber (FMU-204I, Fukushima) used in the characterization system. It is able to programmably control the temperature inside the chamber. We can set the temperature in steps of 0.5°C and the time interval in steps of five minutes. The temperature is measured by using an external temperature recorder (TR-71Ui, T&D) read out via a PC. It takes about 30 minutes that the temperature inside the chamber becomes stable. The chamber will operate at 15°C for one hour, 20°C for one hour, and 25°C for one hour in the



(a) PCB for single channel MPPC. (See Appendix A for the detail of the wiring.)

(b) PCB for MPPC array.

Figure 4.6: Pictures of PCB for MPPCs.

measurement of MPPCs.

4.2.3 Printed circuit board fixing MPPCs

Printed circuit board (PCB) is newly designed and used to fix MPPCs in the chamber. The PCBs have connectors for flat cables to read out signal of MPPC by using EASIROC module. The pictures of PCB are shown in Fig 4.6. Figure 4.6a shows a PCB on which 32 single channel MPPCs can be attached. Sleeves (PD-13, Mac8) are mounted on the PCB, where leads of MPPC are inserted. The signals of single channel MPPC are read out via IDC connector (HIF3BA-34PA-2.54DS, Hirose). Figure 4.6b shows a PCB on which array of 32 channel MPPCs can be attached. Connectors (from Hirose, FH12A-30S-0.5SH for common cathode array and FH12A-36S-0.5SH for independent cathode array, respectively) are mounted on the PCB, where FPC cables of MPPC are inserted. The signals of MPPC array are read out via IDC connector (HIF3BA-34PA-2.54DSA, Hirose).

4.2.4 Light source

A light source is used in the measurement of the gain and relative PDE. Chip LEDs (VLMB1300-GS08, Vishay) are used for the light source to make light intensity uniform. Figure 4.7 shows a schematic of the light source. A NIM level signal is amplified by an LED driver and used to flash LEDs. Figure 4.8 shows a schematic of the LED driver. The light intensity is adjustable by changing the width of the NIM level signal.

4.2.5 Support structure

A support structure is designed to fix PCBs for MPPC and the light source as shown in Fig. 4.9. The size of whole structure is $540 \times 300 \times 390 \text{ mm}^3$. Some parts are made of aluminum and the others are made of polyoxymethylene. The PCBs are attached on the bottom part, and the light source is attached on the top part. The support structure can be used when measuring both single channel and array of MPPC by replacing some parts on the bottom. Two single channel

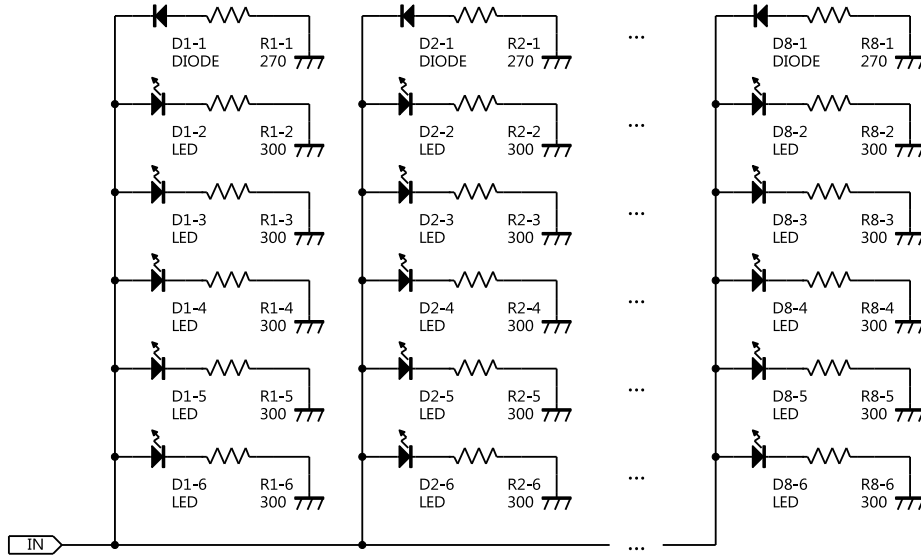


Figure 4.7: A Schematic of the light source. (It is the first version and modified later. See Section 4.4.1.)

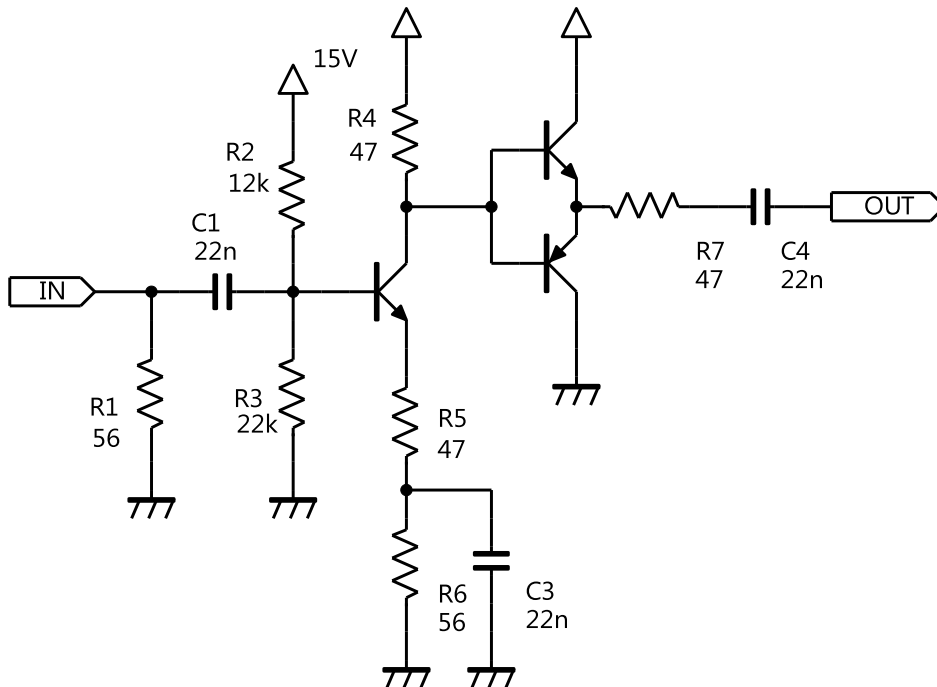


Figure 4.8: A schematic of the LED driver.

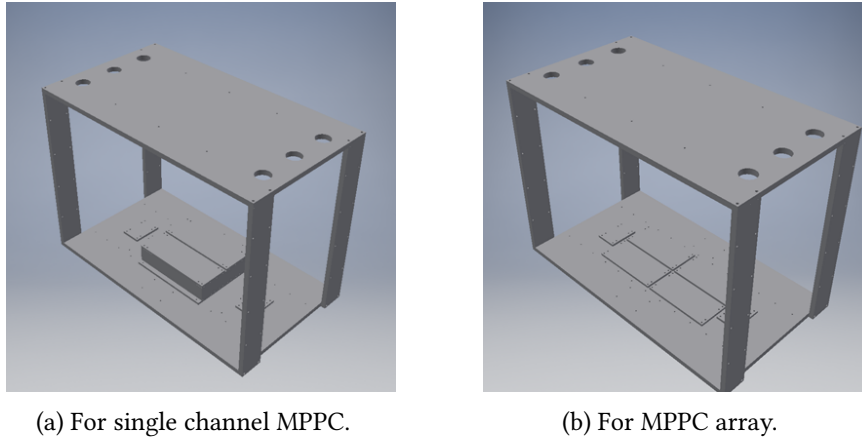


Figure 4.9: Design of the support structure.

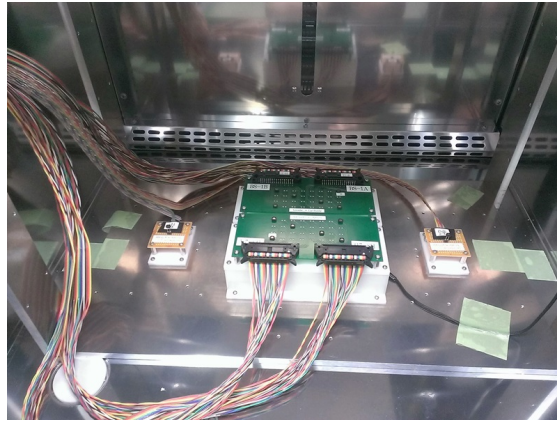


Figure 4.10: Picture when measuring single channel MPPCs.

MPPCs for the reference are placed beside of the MPPCs for the measurement. The MPPC for the reference are also read out by using EASIROC module via a flat cable.

When measuring single channel MPPCs, two PCBs for single channel MPPC are placed and 64 channels are measured simultaneously. When measuring MPPC arrays, four PCBs for MPPC array are placed and 128 channels are measured simultaneously. The number of channels measured simultaneously are limited by the size of the temperature chamber and the uniformity of the light source.

4.3 Measurement method

The procedure of the data acquisition (DAQ) is following.

1. Set MPPCs for the measurement on the corresponding PCB
2. Set the PCBs on the bottom of the support structure
3. Connect the PCBs and EASIROC modules via flat cables

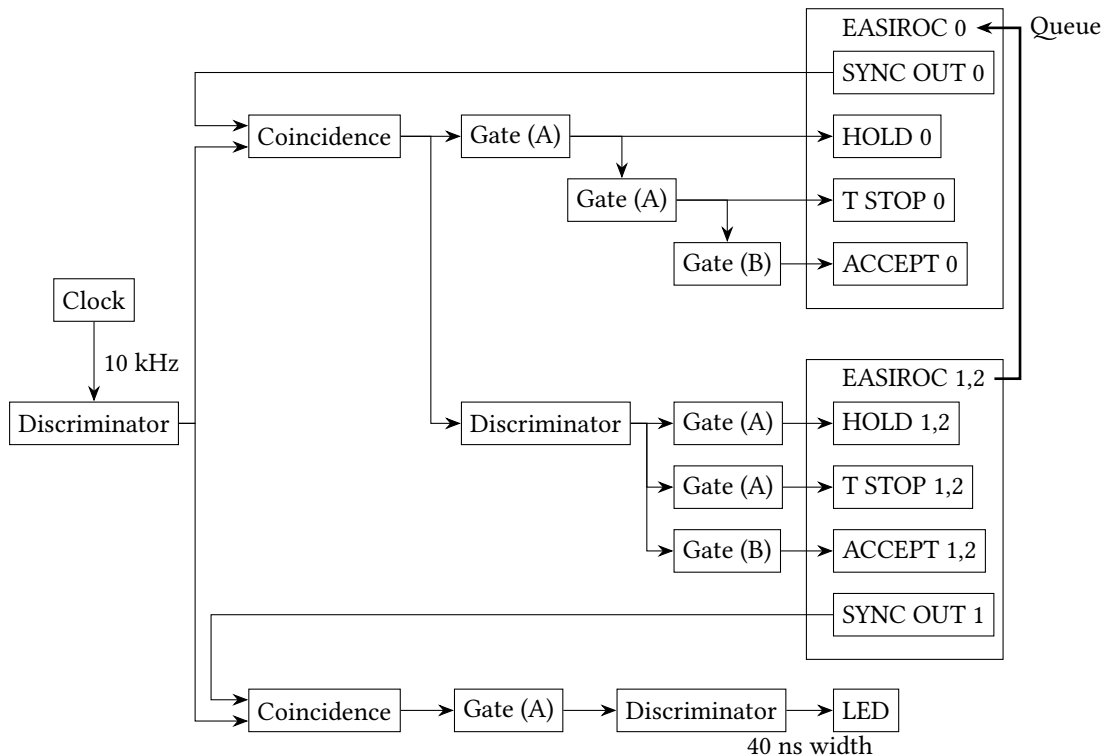


Figure 4.11: Diagram of digital signals when operating characterization system with multiple EASIROC modules.

4. Launch a program of the temperature recorder
5. Launch a test program of DAQ and confirm whether the system works well
6. Launch a main program of DAQ and operation program of the temperature chamber simultaneously
7. Take MPPCs for the measurement out of the temperature chamber

Figure 4.10 shows setting of the MPPCs and the PCBs described in procedure 1 and 2.

Three EASIROC modules are used; one called EASIROC 0 operates MPPCs for the reference and the others called EASIROC 1 and 2 operates MPPCs for the measurement. The EASIROC 2 is not used when measuring single channel MPPCs, since only 64 channels are measured simultaneously. The SYNC OUT output of EASIROC 0 switches on and off of HOLD, T STOP, and ACCEPT signal input in order to synchronize DAQ of each EASIROC module. The SYNC OUT output of EASIROC 1 switches on and off of the light source. The diagram of digital signals when operating the system is shown in Fig. 4.11. The bias voltage applied to MPPCs for the measurement changes ten times in steps of 0.2 V, while the constant over voltage of 3.5 V is applied to MPPCs for the reference. The flow of the DAQ program described in procedure 6 is following.

1. Wait until the temperature inside the chamber becomes stable

2. Increase the bias voltage applied to MPPCs
3. Set the bias voltage
4. Make EASIROC 1 switch on the light source
5. Make EASIROC 1 and 2 enter DAQ mode and push queue to make EASIROC 0 switch on SYNC OUT output
6. Make EASIROC 0 pop queue, enter DAQ mode, and switch on SYNC OUT output to let DAQ start
7. Make EASIROC 1 switch off the light source and take DAQ in the same way as 5 and 6
8. Return to 3, set the bias voltage to next value, and repeat ten times
9. Return to 1, wait until the temperature inside the chamber becomes next value, and repeat three times

4.4 Performance of the characterization system

4.4.1 Light intensity

Uniformity of the light intensity

It is important that the light intensity is uniform and stable for the measurement of the PDE. The spacial distribution of the light intensity was measured by using 64 single channel MPPCs. The layout mapping of 64 single channel MPPCs is shown in Fig. 4.12. First, the gain and the number of detected photons were measured by using the first version of the light source following the method described in Section 4.3. 30,000 events were taken in each over voltage at 20°C. The gain and the number of detected photons of one MPPC are shown in Fig. 4.13. Then, let the light intensity at the position of each MPPC be the number of photons detected by each MPPC with 3.5 V over voltage applied, which is calculated by using a fitted linear function. Figure 4.14 shows the distribution of the light intensity. As shown in Fig. 4.14a, more than 20% asymmetry of the light intensity is seen in the direction of the x axis. After some investigation, it was found that the difference of path length of the circuit from pulse input to each LED causes the difference of pulse shape at each LED, which resulted in the asymmetry of the light intensity. We redesigned the light source based on this result.

The second version of the light source was designed to have four chip LEDs and the same path length of the circuit. Figure 4.15 shows the spacial distribution of the light intensity when using the second version of the light source. The better uniformity of the light intensity was achieved than the first version of the light source. The ratio of the root mean square (RMS) to the mean value is 2.1%, which includes an individual difference of 64 MPPCs.

Stability of the light intensity

The stability of the light intensity was measured by using the second version of the light source. The gain and the number of detected photons were measured ten times at interval of 30 seconds. In this study, we analyzed the data with and without the correction by using MPPCs for

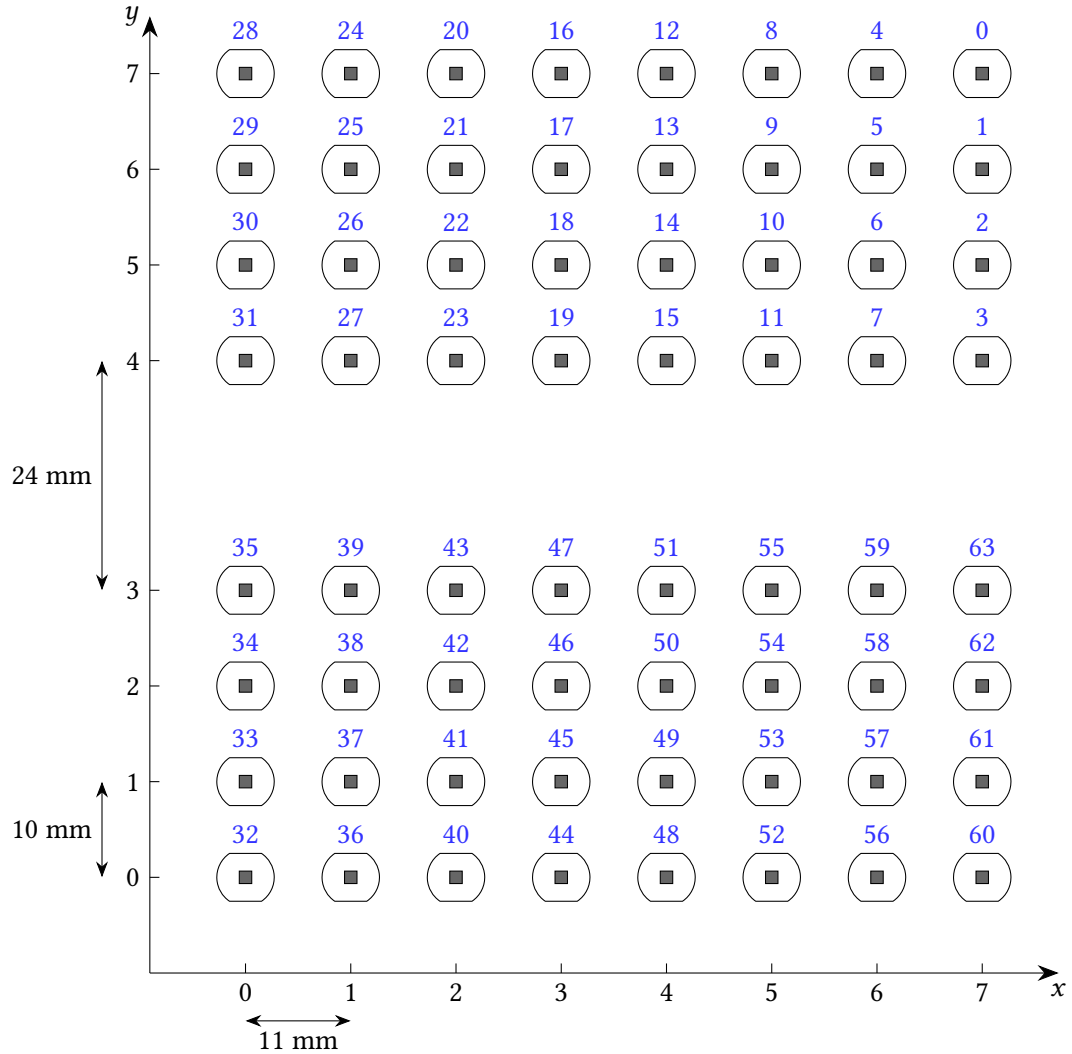
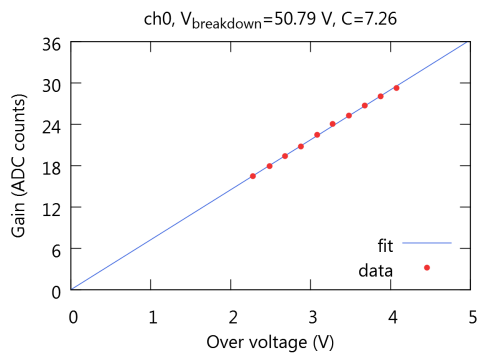
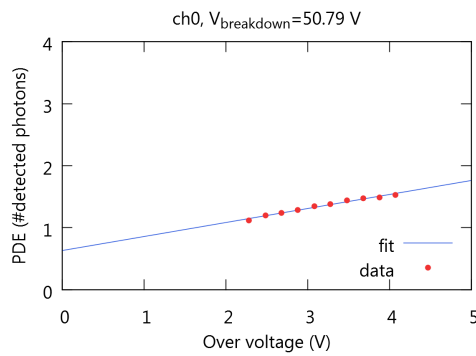


Figure 4.12: The layout mapping of 64 single channel MPPCs. The x and y axes correspond to plots of the spatial distribution. The positions of $y = 3$ and $y = 4$ are at a distance of 24 mm because the MPPCs of $y = 0, 1, 2, 3$ are set in one PCB and the MPPCs of $y = 4, 5, 6, 7$ are set in another PCB. Gray squares are photosensitive area of $1.3 \times 1.3 \text{ mm}^2$. Blue texts are readout channels of the EASIROC module.

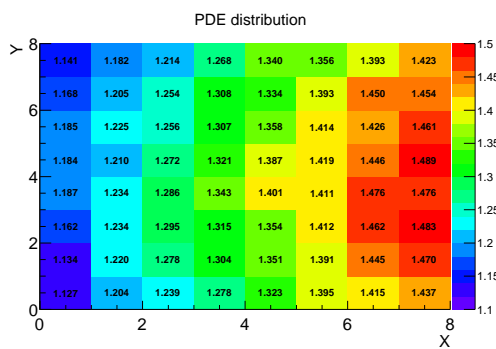


(a) The gain in units of ADC counts of the EASIROC module.

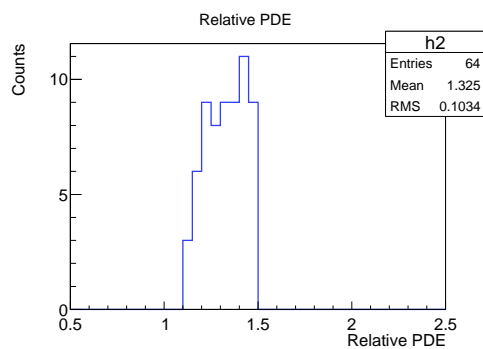


(b) The number of detected photons.

Figure 4.13: The gain and the number of detected photons of one MPPC. Red dots are the measured data and blue lines are fitted function.



(a) The spacial distribution of the light intensity.



(b) The histogram of the light intensity.

Figure 4.14: The distribution of the light intensity in units of the number of detected photons when using the first version of light source.

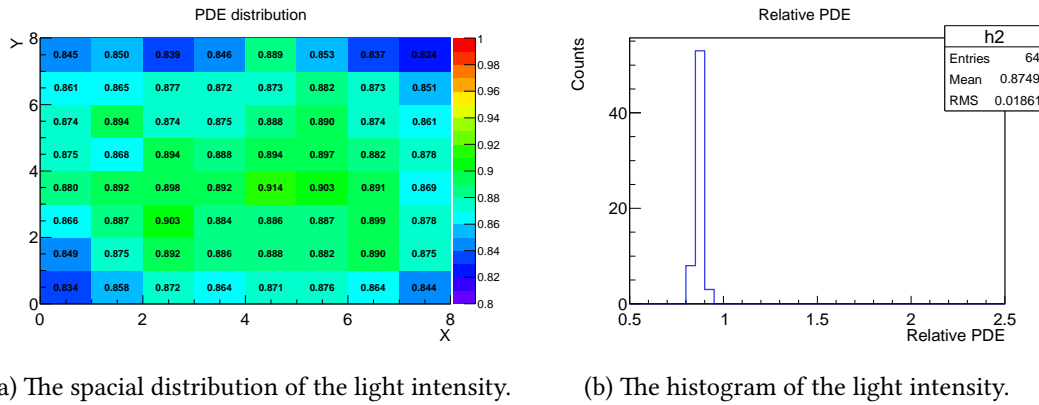


Figure 4.15: The distribution of the light intensity in units of the number of detected photons when using the second version of light source.

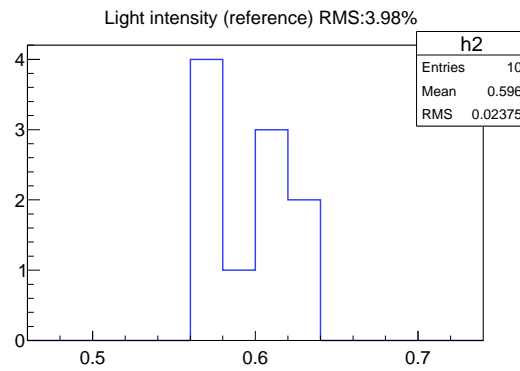


Figure 4.16: The fluctuation of the mean of the number of photons detected by two MPPCs for the reference. The ratio of RMS to mean of ten times measurement is 4.0%.

the reference. When applying the correction, the light intensity is calculated as the ratio the number of photons detected by the MPPC for the measurement to the light intensity for the reference:

$$\text{Light intensity with the correction} = \frac{\text{The number of photons detected by the MPPC for the measurement}}{\text{The light intensity for the reference}}, \quad (4.1)$$

in order to avoid the fluctuation of the light intensity. Let the fluctuation of the light intensity be the ration of RMS to the mean of ten times measurement.

Two MPPCs were used for the reference with 3.5 V over voltage applied. The light intensity for the reference is calculated as the mean of the number of photons detected by each of two MPPCs for the reference. Figure 4.16 shows the mean of the light intensity for the reference. The fluctuation of the light intensity for the reference is 4.0%.

The stability of the light intensity at the position of MPPCs for the measurement is shown in

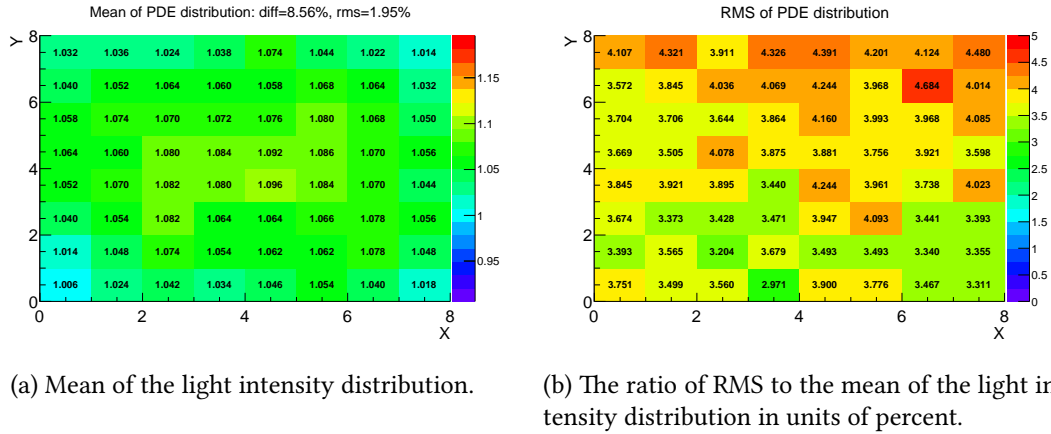


Figure 4.17: The light intensity distribution of ten times measurement without the correction by using the light intensity for the reference. Figure 4.17a shows the mean of ten times measurement in each channel. Figure 4.17b shows the ratio of RMS to the mean of ten times measurement in each channel.

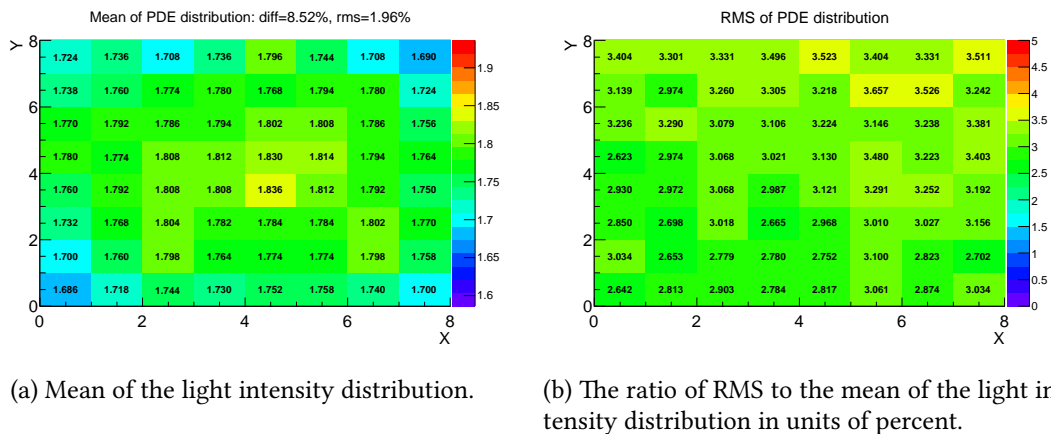
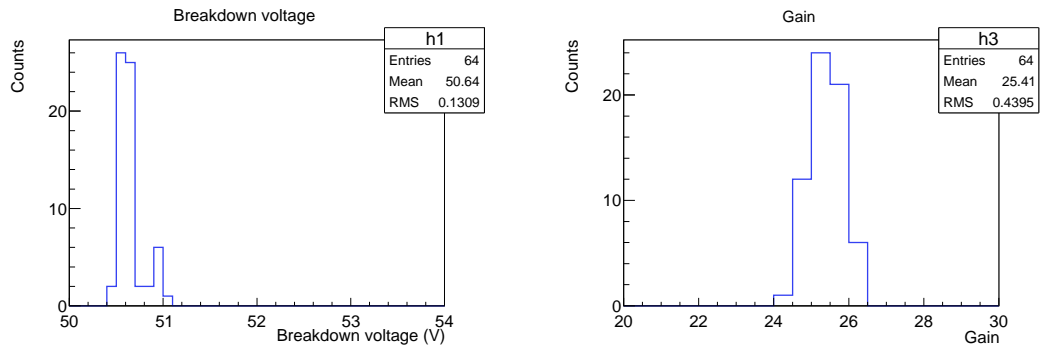
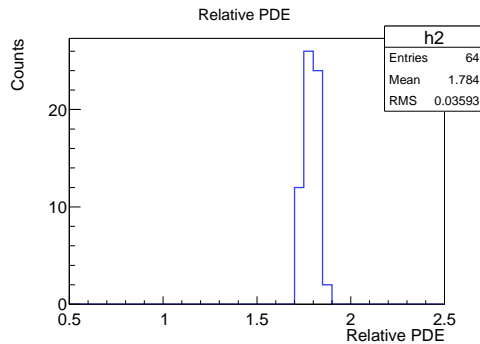


Figure 4.18: The light intensity distribution of ten times measurement with the correction by using the light intensity for the reference. Figure 4.18a shows the mean of ten times measurement in each channel. Figure 4.18b shows the ratio of RMS to the mean of ten times measurement in each channel.



(a) Breakdown voltage.

(b) Gain in units of ADC counts of the EASIROC moduel measured at 3.5 V over voltage.



(c) The number of photons detected by MPPCs with 3.5 V over voltage applied.

Figure 4.19: Performance of 64 MPPCs.

Fig. 4.17 and 4.18. Figure 4.17 shows the light intensity distribution of ten times measurement without the correction by using the light intensity for the reference. The fluctuation of the light intensity for the measurement without the correction is 3.8%. Figure 4.18 shows the light intensity distribution of ten times measurement with the correction by using the light intensity for the reference. The fluctuation of the light intensity for the measurement with the correction is 3.1%. The correction by using the light intensity for the reference reduces the fluctuation of the light intensity from 3.8% to 3.1%. Meanwhile, the cause of the fluctuation of the light intensity is unknown so far. It can be uncertainty when measuring the large number of MPPCs. The further improvement of uniformity and stability of the light intensity is desired.

4.4.2 Performance of 64 MPPCs

Figure 4.19 shows the performance of 64 single channel MPPCs. The gain and the number of detected photons of 64 MPPCs are successfully measured simultaneously. The performance of 64 MPPCs are uniform as the ratio of the RMS to the mean value of the gain is 1.7% and that of the number of detected photons is 2.0%.

Chapter 5

Future prospects and summary

5.1 Future prospects

The characterization system described in the previous chapter is still under development. Several works need to be completed before we can start the characterization of MPPCs. In the following, prospects of future work are explained.

5.1.1 Light intensity

The uniformity of the light intensity of 2.0% was achieved including individual difference of 64 MPPCs. The stability was evaluated to be around 3% by repeating the measurement ten times. The further improvement of uniformity and stability of the light intensity is desired. In addition, the uniformity of the light intensity should be measured by using the same MPPC in different positions.

5.1.2 Dark noise and optical crosstalk

The method of measuring the dark noise rate and optical crosstalk by using the scaler in the EASIROC module is not established yet. The idea of measuring the dark noise rate and optical crosstalk is following.

1. Measure the gain with the light source on
2. Set the threshold of the discriminator to 0.5 p.e. level calculated from the measured gain
3. Take data with the light source off
4. Set the threshold of the discriminator to 1.5 p.e. level calculated from the measured gain
5. Take data with the light source off

It is necessary that the relationship between the gain and the threshold of the discriminator is measured in advance. Once the method is established, the dark noise and optical crosstalk are measured following the measurement of the gain and relative PDE.

5.1.3 Temperature scan

The main program of DAQ is not adopted to temperature scan yet. The function will be implemented to synchronize the DAQ program with the program of temperature controlled chamber in the way that the DAQ program starts DAQ after the specified time has passed.

5.1.4 Measurement of the MPPCs used in the WAGASCI detector

The performance of the MPPCs used in the WAGASCI detector will be measured successively once the whole required function is implemented in the characterization system. We will confirm whether the MPPCs have good performance to be used in the WAGASCI detector.

It takes three hours to run the whole measurement, which is determined by the performance of the temperature controlled chamber. We assume that the measurement is carried out three times a day. In this case, it takes 15 days to measure 2750 single channel MPPCs and 14 days to measure 168 arrays of MPPC (i.e. 5376 channels). In total, 29 days are necessary to complete the measurement of MPPCs used in the WAGASCI detector.

5.2 Summary

The WAGASCI experiment aims to measure the charged current cross section ratio between H_2O and CH with 3% accuracy by using the J-PARC neutrino beam. The performance of the newly developed MPPC has been measured. The optical crosstalk suppression type MPPCs used in the WAGASCI detector have an order of magnitude lower dark noise rate and optical crosstalk than earlier devices, and can be operated with higher over voltage, which also results in higher PDE. We developed an array of 32 MPPCs for a compact readout with a large number of channels.

A characterization system to measure a large number of MPPCs has been developed because the WAGASCI detector will have a large number of readout channels to be 8000. The gain, relative PDE, dark noise rate, and optical crosstalk will be measured for different temperature and over voltage. The performance of 64 single channel MPPCs or four arrays of MPPC (i.e. 128 channels) will be simultaneously and automatically measured by using the characterization system. The measurement of the gain and relative PDE of 64 MPPCs with operating MPPCs for the reference already succeeded. Once the DAQ program and the light source are improved, the performance of all MPPCs used in the WAGASCI detector will be measured in the future.

Appendix A

Wiring of the PCB for single channel MPPC

This appendix presents the wiring of the PCB for single channel MPPC described in Section 4.2.3. Figure A.1 shows the wiring of anodes. Figure A.2 shows the wiring of cathodes.

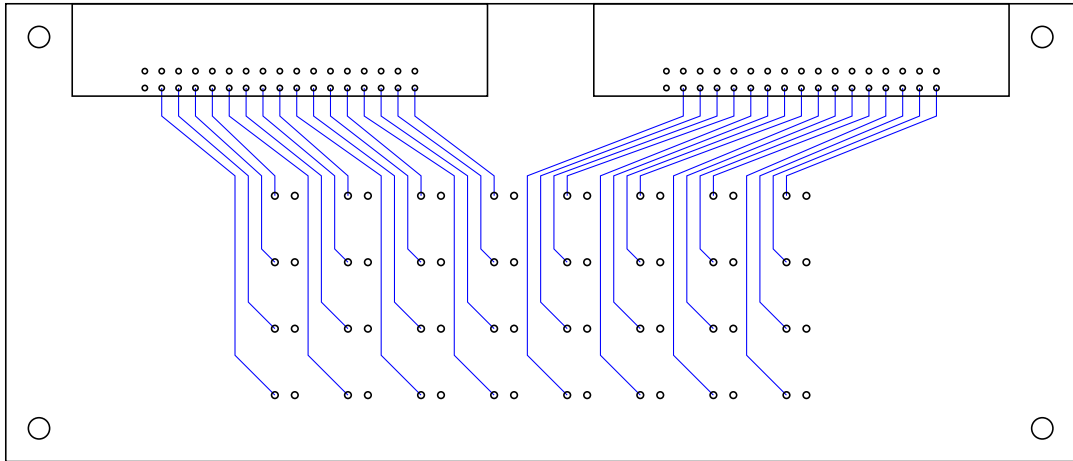


Figure A.1: The wiring of anodes.

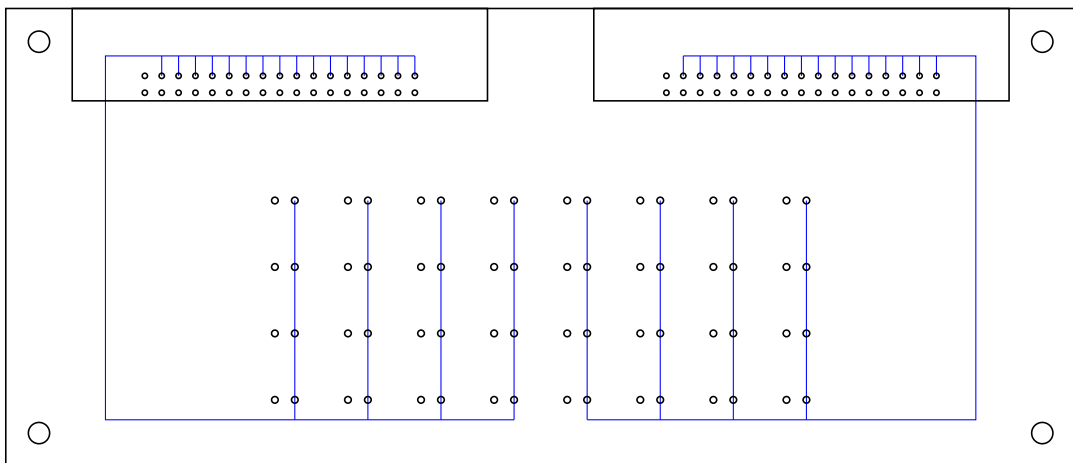


Figure A.2: The wiring of cathodes.

Bibliography

- [1] Y. Fukuda *et al.* (Super-Kamiokande Collaboration), Phys. Rev. Lett. **81**, 1562 (1998), [arXiv:hep-ex/9807003](#).
- [2] Q. R. Ahmad *et al.* (SNO Collaboration), Phys. Rev. Lett. **87**, 071301 (2001), [arXiv:nucl-ex/0106015](#).
- [3] B. Pontecorvo, Sov. Phys. JETP **6**, 429 (1957), [Zh. Eksp. Teor. Fiz.33,549(1957)].
- [4] B. Pontecorvo, Sov. Phys. JETP **7**, 172 (1958), [Zh. Eksp. Teor. Fiz.34,247(1957)].
- [5] Z. Maki, M. Nakagawa, and S. Sakata, Prog. Theor. Phys. **28**, 870 (1962).
- [6] B. Pontecorvo, Sov. Phys. JETP **26**, 984 (1968), [Zh. Eksp. Teor. Fiz.53,1717(1967)].
- [7] K. Abe *et al.* (T2K Collaboration), Nucl. Instrum. Meth. **A659**, 106 (2011), [arXiv:1106.1238](#).
- [8] Y. Fukuda *et al.* (Super-Kamiokande Collaboration), Nucl. Instrum. Meth. **A501**, 418 (2003).
- [9] K. Abe *et al.* (T2K Collaboration), Phys. Rev. Lett. **107**, 041801 (2011), [arXiv:1106.2822](#).
- [10] K. Abe *et al.* (T2K Collaboration), Phys. Rev. **D85**, 031103 (2012), [arXiv:1201.1386](#).
- [11] K. Abe *et al.* (T2K Collaboration) (2015), [arXiv:1512.02495](#).
- [12] K. Abe *et al.* (T2K Collaboration), PTEP **2015**, 043C01 (2015), [arXiv:1409.7469](#).
- [13] K. Abe *et al.* (T2K Collaboration), Phys. Rev. **D91**, 072010 (2015), [arXiv:1502.01550](#).
- [14] K. Abe *et al.* (T2K Collaboration), Phys. Rev. Lett. **112**, 061802 (2014), [arXiv:1311.4750](#).
- [15] T. Koga *et al.*, JPS Conf. Proc. **8**, 023003 (2015).
- [16] T. Koga, *Research and development of a new neutrino detector for precise measurement of neutrino-nucleus cross sections*, Master's thesis, the University of Tokyo (2015).
- [17] K. Abe *et al.* (T2K Collaboration), Phys. Rev. **D90**, 052010 (2014), [arXiv:1407.4256](#).
- [18] N. Chikuma *et al.*, PoS **FPCP2015**, 069 (2015).
- [19] N. Chikuma, *Research and development of magnetized muon detector and readout electronics for a neutrino cross section experiment*, Master's thesis, the University of Tokyo (2016).

- [20] Hamamatsu Photonics K. K., *MPPC and MPPC module for precise measurement* (2015).
- [21] Hamamatsu Photonics K. K., *Opto-semiconductor 2014* (2014).
- [22] K. Yamamoto, K. Yamamura, K. Sato, S. Kamakura, T. Ota, H. Suzuki, and S. Ohsuka, PoS **PD07**, 004 (2006).
- [23] M. Yokoyama *et al.*, Nucl. Instrum. Meth. **A610**, 128 (2009), [arXiv:0807.3145](https://arxiv.org/abs/0807.3145).
- [24] R. Honda, K. Miwa, I. Nakamura, M. Tanaka, K. Yoshimura, T. Uchida, and M. Ikeno, PoS **PhotoDet2012**, 031 (2012).